

PLRP2 selectively localizes synaptic membrane proteins via acyl-chain remodeling of phospholipids

Hideaki Kuge¹*, Izumi Miyamoto¹, Ken-ichi Yagyu², and Koichi Honke¹*

¹Department of Biochemistry, Kochi University Medical School, Nankoku, Kochi, Japan, and ²Science Research Center, Kochi University Medical School, Nankoku, Kochi, Japan

Abstract The plasma membrane of neurons consists of distinct domains, each of which carries specialized functions and a characteristic set of membrane proteins. While this compartmentalized membrane organization is essential for neuronal functions, it remains controversial how neurons establish these domains on the laterally fluid membrane. Here, using immunostaining, lipid-MS analysis and gene ablation with the CRISPR/Cas9 system, we report that the pancreatic lipase-related protein 2 (PLRP2), a phospholipase A1 (PLA1), is a key organizer of membrane protein localization at the neurite tips of PC12 cells. PLRP2 produced local distribution of 1-oleoyl-2-palmitoyl-PC at these sites through acyl-chain remodeling of membrane phospholipids. The resulting lipid domain assembled the syntaxin 4 (Stx4) protein within itself by selectively interacting with the transmembrane domain of Stx4. The localized Stx4, in turn, facilitated the fusion of transport vesicles that contained the dopamine transporter with the domain of the plasma membrane, which led to the localized distribution of the transporter to that domain. These results revealed the pivotal roles of PLA1, specifically PLRP2, in the formation of functional domains in the plasma membrane of neurons. In addition, our results suggest a mode of membrane organization in which the local acyl-chain remodeling of membrane phospholipids controls the selective localization of membrane proteins by regulating both lipid-protein interactions and the fusion of transport vesicles to the lipid domain.

Supplementary key words glycerophospholipids • membrane lipids • membranes/fluidity • phospholipases • phospholipid remodeling • acyl-chain configuration • phospholipase A1 • dopamine transporter • syntaxin • pancreatic lipase-related protein 2

Many cells have a plasma membrane that contains various functionally distinct domains (1). Neurons are one notable example of such cells, as they carry specialized domains at the presynaptic, postsynaptic, and soma membranes, as well as at different regions of the axon. This compartmentalized membrane organization is essential for the neuronal transmission of information directionally and for the formation of elaborate neural circuits in the brain. To implement these functionally

different domains, cells deliver a customized set of membrane proteins to each region. In addition, neurons must selectively confine these proteins within the limited regions, to maintain the domains (2), despite the fact that membrane proteins are, in general, laterally mobile over the cell surface (3). Although these phenomena have been studied well, the mechanism underlying these processes remains unclear.

Transport vesicles carry the membrane proteins to the target region of the membrane (4). Soluble *N*-ethylmaleimide-sensitive factor attachment protein receptor (SNARE) proteins play key roles in the target specification of these vesicles, especially at the docking stage of the vesicles to the target membranes. In this model, each transport vesicle is labeled with a member of vesicular-SNARE proteins (v-SNAREs) corresponding to its destination, and the target region of the membrane is marked with a member of the target-SNARE proteins (t-SNAREs). Correct matching of the t-SNARE to the v-SNARE on the vesicles is a prerequisite for the fusion of the two membranes and for the delivery of the cargo proteins to the target membrane (5). This model is widely accepted as the core mechanism underlying target selection by transport vesicles. However, the manner in which the t-SNARE locally marks the target region of the membrane remains unknown (6).

Phospholipids are the base components of biomembranes. In addition to variation in their hydrophilic portion, phospholipids comprise various molecular species with different combinations of acyl chains, which constitute the hydrophobic core of the lipid bilayer (7, 8). This acyl chain variety is produced by a process called “acyl chain remodeling” or “Lands cycle” (9). In this process, one of the two acyl chains in a phospholipid molecule is cleaved by phospholipase A, followed by the attachment of a different fatty acid to the lysophospholipid product by acyltransferase or transacylase. Although many of the enzymes involved in this process have been documented (10, 11), little is known about the cellular functions of the acyl chain variation.

In relation to the functions of the acyl chain variation, we previously showed that 1-oleoyl-2-palmitoyl-PC (OPPC), which is a rare molecular phospholipid species, is locally concentrated at the peri-synaptic area of several neuronal cells through acyl chain remodeling at the *sn*-1 site of PC and is implicated in its involvement in the local confinement of

This article contains [supplemental data](#).

*For correspondence: Hideaki Kuge, kugeh@kochi-u.ac.jp; Koichi Honke, khonke@kochi-u.ac.jp



membrane proteins (12). However, the nature of the enzymes that carry out this remodeling or their roles in the control of the allocation of membrane proteins remains unclear. In this article, we describe a phospholipase A1 (PLA1) enzyme that is responsible for the regional distribution of OPPC. Moreover, we show its involvement in the vesicular delivery mechanism and in the local organization of the plasma membrane.

MATERIALS AND METHODS

Cell culture

PC12 cells were cultured as described previously (12). The cells were treated with 50 ng/ml nerve growth factor (NGF) (Alomone Labs, N130) for 48 h or specified periods to induce neuronal development. COS7 and HeLa cells were cultured in DMEM (WAKO, 044-29765) with 10% FBS on glass-bottom dishes (Iwaki) for immunostaining studies.

Antibody to PLRP2

An antibody to pancreatic lipase-related protein 2 (PLRP2) (Abcam, ab37599) was used for the initial screening. For the figures presented in this study, an in-house generated rabbit antiserum to rat PLRP2 was prepared via immunization with GST-PLRP2 (AA236-482) produced in *Escherichia coli*.

DNA transfection

DNA lipofections into PC12 cells were performed using EZT-PC12 (EZ Biosystems) with DNA/reagent = 2 µg/2.8 µl in 3 cm dishes. The culture medium was replaced at 6 h after transfection. DNA lipofections into COS7 cells were performed using Lipofectamine 3000 (Thermo) or ViaFect (Promega), as described in the manufacturer's instructions. Cells were fixed for observation 16–24 h after the DNA transfections.

Immunofluorescence staining procedures

PC12 cells were washed with PBS and fixed with 4% paraformaldehyde in 0.1 M sodium phosphate (pH 7.2) for 15 min, and then with methanol at –20°C for 30 min. The fixed cells were preincubated with 10% heat-inactivated goat serum in PBS for 1 h before adding the primary antibodies. These cell preparations were incubated with the primary antibodies for 12 h at 4°C. The dilution conditions for the antibodies were as follows: the anti-PLRP2 (generated in-house), anti-Thy-1 (Millipore, MAB1406), anti-dopamine transporter (DAT) (Proteintech, 22524-1-AP), anti-syntaxin 1A (Stx1A) (GeneTex, GTX113559), and anti-syntaxin 4 (Stx4) (GeneTex, GTX114806) antibodies were used at 1:100 dilution; and mAb#15 was used at 0.3 µg/ml. All antibodies were diluted in 5% skim milk containing 1% goat serum in PBS. After washing the primary antibody with PBS, the cells were stained with 5,000-fold-diluted secondary antibodies: Alexa 488-labeled (Fig. 2C), Alexa 555-labeled (Figs. 1A, 2A, 3C, 4A, B, and D, 9A), or Alexa 633-labeled (Figs. 3A and B, 4C) antibody to mouse IgM and CF430 (Biotium) (Figs. 3C, 4D); or Alexa 488-labeled (Figs. 1A, 2A, 3A and B, 4A–C, 9A and B) antibody to rabbit IgG and Alexa 555-labeled antibody to mouse IgG (Fig. 2A) in 10% goat serum in PBS. In the case of COS7 and HeLa cells, cells were fixed as described above and then treated with 0.1% saponin (Sigma, S4521) in PBS for 10 min. After washing the cells with PBS, the cells were preincubated with 1% BSA in PBS for 1 h before adding the primary antibodies. The cell preparations were incubated with the primary antibodies for 12 h at 4°C. The dilution conditions for the antibodies were as follows: mAb#15, 0.3

µg/ml (Figs. 2C, 11C); anti-HA (MBL, M180-3), 1:1,000; anti-RFP (MBL, M165-3), 1:1,000; and anti-Myc (GeneTex, GTX115046), 1:1,000 (Fig. 11C) in 5% milk in PBS. After washing the primary antibody with PBS, the cells were stained with 5,000-fold-diluted secondary antibodies: Alexa 488-labeled antibody to mouse IgM (Invitrogen) (Fig. 2C) or DyLight 405-labeled (Rockland) antibody to mouse IgM (Jackson Immuno Research, 715-475-020), Alexa 488-labeled antibody to mouse IgG 2b (Invitrogen), Alexa 555-labeled antibody to mouse IgG 1 (Invitrogen), and Alexa 635-labeled antibody to rabbit IgG (Invitrogen) (Fig. 11C) in 1% BSA in PBS. The cells were observed with a confocal fluorescence microscope with Nomarski optics (Olympus FV10).

Western blotting

For the analysis of PLRP2 protein expression, cell lysates (15 µg protein each) in SDS sample buffer containing 10% β-mercaptoethanol were heat denatured and separated by SDS-PAGE on 7.5% gels. The separated proteins were transferred to PVDF membranes, blocked with 5% milk in TBST (blocking buffer), and probed with an in-house-generated antibody to PLRP2 (1:100,000) in blocking buffer. After washing the membrane with TBST, a HRP-conjugated antibody to rabbit IgG (1:100,000; Promega, W4011) in blocking buffer was applied. The membranes were developed with HRP-substrate (Millipore, WBKLS0500) and recorded on X-Ray films. For the detection of Stx4 expression, 10% gels and the antibody to Stx4 (as above; 1:10,000) in blocking buffer were used. For DAT expression, the antibody to DAT (Proteintech, 22524-1-AP) was diluted (1:10,000) in an immunoreaction enhancer solution (TOYOBO, NKB-101). For the analysis of DAT expression in COS7 cells, the cells in 12-well plates were lysed 20 h after the transfection using SDS-sample buffer containing 10% β-mercaptoethanol. After blotting, the membrane was probed with an antibody to Myc (MBL, 192-3; 1:500) in blocking buffer. After washing the membrane with TBST, a HRP-conjugated antibody to mouse IgG (Promega, W4021) in blocking buffer (1:100,000) was applied. The membranes were developed with the HRP-substrate and recorded using a CCD camera (LAS4000, Fuji Film). The intensity of the Myc-DAT bands from different expression constructs was quantified using the Image Quant software (Fuji Film).

Oligo DNAs used in this study

Oligo DNAs used in this study are described in supplemental Table S1.

RT-PCR analyses

Total RNA was isolated using an RNA isolation kit (Roche, 11828665001) from three independent pairs of about 5×10^5 PC12 cells incubated without or with NGF for 48 h. The cDNA was produced by superscript II enzyme (Thermo) using 250 ng of random primer on 2 µg each of total RNA according to the manufacturer's instructions. For the quantification of the *plrp2* cDNA, PCR was performed using oligo DNAs PLRP2 502 fwd and PLRP2 804 rev, KOD plus neo DNA polymerase (TOYOBO), 34 cycles of 98°C for 10 s, and 68°C for 20 s. For glycerol-3-phosphate dehydrogenase (G3PDH) amplification, PCR was performed using G3PDH fwd and G3PDH rev, the same enzyme, and 26 cycles of the same reaction conditions. The amplified cDNA was separated in 2% agarose gels and quantified with a CCD camera.

Expression constructs

The cDNA for rat *plrp2* was prepared from total RNA isolated from PC12 cells by RT-PCR using primer sets #1 and #2, followed by cloning into a *KpnI/NotI* digest of pCMV SPORT6 vector (construct A). The obtained sequence matched completely that of rat

plrp2 (*pnliprp2*: NCBI NM_057206). CMV-*plrp2* (wild-type)-*DsRed* fusion (construct B) was assembled by combining the following four PCR fragments into a *HindIII*/*PmeI* digest of pcDNA3.1 with Gibson assembly (NEB): fragment #1, primers #3 and #4 applied on construct A; fragment #2, primers #5 and #6 applied on construct A; fragment #3, primers #7 and #8 applied on a plasmid with *DsRed*; and fragment #4, primers #9 and #10 applied on construct A. In this construct, codon #99 of *plrp2* was changed from gaC (Asp) to gaT (Asp), to confer resistance against CRISPR for revertant expression in the PLRP2-KO cells. CMV-*plrp2* (lipase inactive)-*DsRed* fusion (construct C) was produced by substituting Ser (184, agc) with Gly (ggc) and replacing His (295 cac) with Leu (ctc) in the *plrp2* coding region in construct B, by assembling the following three PCR fragments applied on construct B: fragment #1, primers #3 and #11; fragment #2, primers #12 and #13; and fragment #3, primers #14 and #10. CMV-*plrp2* (wild-type)-*mCherry* fusion (construct D) and CMV-*plrp2* (lipase inactive)-*mCherry* fusion (construct E) were prepared by replacing the *DsRed*-HA-FLAG part of constructs B and C, respectively, with *mCherry*, by combining the following three PCR fragments into each construct: fragment #5, primers #6 and #15 applied on construct B; fragment #6, primers #16 and #17 applied on a plasmid with *mCherry*; and fragment #7, primers #10 and #18 applied on construct B.

The cDNAs for rat *stx1A* and *stx4* were prepared from total RNA isolated from PC12 cells by RT-PCR using primer sets #19 and #20 or #21 and #22, respectively, followed by cloning into a *HindIII*/*ApaI* digest of the pcDNA3.1 vector (constructs F and G). The cDNA for *stx1A* matched completely rat *stx1a* (NCBI NM_053788.2). All of the cDNA clones obtained for *stx4* had one substitution at the codon corresponding to Thr 216 (ACG) to Ser (AGC) compared with rat *stx4* (NCBI NM_031125.1). The CMV-HA tag-*Stx4*-IRES-*mCherry* construct (construct H) was assembled into a *SacI*/*BstZ171* digest of pcDNA 3.1 using the following six PCR fragments: fragment #8, primers #23 and #24; fragment #9, primers #25 and #26; fragment #10, primers #27 and #28, all applied on construct G; and fragment #11, primers #29 and #30 applied on a vector with IRES; fragment #12, primers #31 and #17 applied on construct D; and fragment #13, primers #32 and #33 applied on construct D. In this construct, codon #36 of *stx4* was changed from agC (Ser) to agT (Ser), to confer resistance against CRISPR for revertant expression in the *Stx4*-KO cells. The *mCherry*-transmembrane domain (TMD) (*Stx1A* amino acids 253–287) fusion construct was assembled on the *HindIII* digest of construct D using the following two PCR fragments: fragment #16, primers #34 and #17 applied on construct D; and fragment #17, primers #35 and #36 applied on construct F. The *mCherry*-TMD (*Stx4* amino acids 263–298) (construct I) fusion construct was assembled on the *HindIII* digest of construct D using the following two PCR fragments: fragments #16 and #18: primers #37 and #38 applied on construct G. The *mCherry*-TMD (*Stx4* 290IF) construct (construct L) was assembled on the *SbfI*/*PmeI* digest of construct I using the following two PCR fragments: fragment #27, primers #51 and #52 applied on construct I; and fragment #28, primers #53 and #10 applied on construct I. The CMV-*mCherry* alone construct (construct J) was assembled into the *HindIII* digest of construct D using the following two PCR fragments: fragments #16 and #19, primers #39 and #38, applied on construct I.

The cDNAs for DAT were prepared from total RNA isolated from PC12 cells by RT-PCR using the primer sets #40 and #41, followed by cloning into an *EcoRI*/*NotI* digest of the pcDNA3.1/V5-His A vector (construct K). The obtained sequence matched completely the rat *slc6a3* (DAT: NCBI NM_012694.2). In Fig. 7, construct #1 was construct J. Construct #2 was assembled into a *NheI*/*Bstz171* digest of construct J using the following three PCR fragments: fragment #20, primers #42 and #43 applied on construct H; fragment #21, primers #44 and #45 applied on con-

struct K; and fragment #22, primers #46 and #47 applied on construct H. Construct #3 was assembled into a *NheI*/*Bstz171* digest of construct D using the three PCR fragments that were used to build construct #2. Construct #4 was assembled into a *NheI*/*Bstz171* digest of construct J using the following three PCR fragments: fragment #23, primers #42 and #48 applied on construct H; fragment #24, primers #49 and #28 applied on construct H; and fragment #25, primers # 50 and #47 applied on construct #2. Construct #5 was assembled into a *NheI*/*Bstz171* digest of construct #3 using PCR fragment #26, primers #42 and #47 applied on construct #4.

Gene KO by CRISPR/Cas9

The targeting vector for the *plrp2* locus was constructed using a *BsmBI* digest of the LentiCRISPRv2 vector by inserting the duplex of oligo DNAs PLRP2 CRISPR #1 and #2, as described previously (13). For targeting the *stx4* locus, the following oligo DNAs were used: *Stx4* CRISPR #1 and #2. Infectable lentiviruses were produced by transfecting the following three plasmid DNAs into H293T cells using Lipofectamine 2000 (Thermo): one of the targeting vectors, a packaging plasmid (ps PAX2), and an envelope plasmid (pMD2.G). These two plasmids were gifts from Didier Trono (Addgene plasmids #12260 and #12259). After adding the targeting virus to PC12 cells, infected cells were selected with 3 μ g/ml of puromycin for 1 week. The cells were clonally expanded and analyzed regarding genome sequence and the expression of the target proteins.

In situ PLA1 assay

PC12 cells treated with NGF for 48 h were washed with PBS at 37°C, followed by the addition of the PED-A1 substrate (Invitrogen) at 1 μ M. The cells were immediately observed for less than 30 min using a confocal fluorescence microscope with the excitation wavelength set at 488 nm and the emission band pass set between 500 and 600 nm.

Isolation of the neurite fraction

The original PC12 cells and the PLRP2-KO cells (5×10^7 cells each) were cultured in the presence of NGF for 48 h. After washing with PBS at 37°C three times, the cells were washed once with lysis buffer [0.32 M sucrose, 1 mM EDTA, 20 mM HEPES (pH 7.4), and 2 \times complete protease inhibitor mix (Roche, 11 836 145 001)] at 4°C. The cells were collected using rubber scrapers and centrifuged at 200 *g* for 3 min to remove cell bodies, which yielded a pellet of about 0.9 g for each cell type. The supernatants, which were enriched in neurite fragments, were centrifuged at 22,000 *g* for 60 min at 4°C to recover the neurite fraction (NF).

Lipid analysis of the NF

The NF pellets were dissolved in 550 μ l of 5 mM Tris (pH 7.5). The protein content of the NF was measured by Bradford Ultra protein assay (Expedeon, BFU05L) after dissolving a fraction of the NF in 0.1% SDS. Lipids were extracted from 500 μ l of the NF by adding 5 ml of chloroform/methanol (1:1) with mixing by rotation for 12 h. The mix was centrifuged at 4,000 *g* for 10 min to recover the supernatant as the NF lipid fraction. Lipids were evaporated with N₂ gas, dissolved in 250 μ l of chloroform/methanol (2:1), and filtered through a 0.2 μ m filter. A portion of the lipid extract (20 μ l) was separated on a C8 reversed phase column (OS12S03-1546WT, YMC) at 40°C by isocratic elution with 10 mM triethylamine acetate (pH 4) in water/methanol (7:93) at a flow rate of 1 ml/min on a HPLC system (Shimazu, LC-20). OPPC (Sigma; 0.25 g/l, 20 μ l) was also analyzed as an elution marker. The elute fractions (0.5 ml each) were collected for further analysis from the retention time of 10–20 min.

ELISA with mAb#15

A portion of each elute fraction (40 μ l, in triplicate) was applied to 96-well ELISA plates (Immulon 1B, Thermo). The lipid samples were dried at 80°C for 30 min. Subsequently, the plates were blocked with 1% BSA in PBS for 1 h and incubated for 30 min with 0.1 mg/ml mAb#15 in 5% milk in 1% BSA/PBS. After washing with PBS, the secondary antibody [HRP-conjugated antibody to mouse IgM (sc-2064, Santa Cruz Biotechnology), 100,000-fold dilution in 1% BSA, PBS] was added, followed by incubation for 30 min. After washing the plates with PBS, the immunoreactivity was quantified with a chemiluminescent HRP substrate (Millipore) and measured on a luminometer (BioTek, Cytation5).

MALDI-TOF-MS analysis

The lipid samples were mixed with 25 μ M dimyristoylphosphatidylcholine (Sigma, P7930) at a 2:1 ratio and then mixed at a 1:1 ratio with 25 g/l 2,5-dihydroxybenzoic acid (DHB) (Sigma)/DHB-Li (Wako) at a mixing ratio of 9:1 in 1:1 methanol/water, as described previously (12, 14). These samples were analyzed on an ABI SCIEX TOF-TOF 5800 mass spectrometer in positive ion mode. The sum of the peak heights recorded at m/z 760.4 ($M+H^+$), m/z 766.5 ($M+Li^+$), and m/z 782.4 ($M+Na^+$) was compared with that of DMPC to calculate the mole amount of PC (34:1). For MS/MS analysis, collision-induced dissociation fragmentation was performed with a collision energy of 2 kV (15). The content of OPPC and POPC in PC (34:1) was calculated by comparing the peak heights recorded at m/z 425 (A) and at m/z 451 (B) using the following formulas: OPPC = 1.38A - 0.38B, POPC = -0.38A + 1.38B based on the MS/MS fragmentation profile of the OPPC standard (12, 14).

Dopamine uptake assay

PC12 cells treated with NGF for 3 days were washed with HBSS with 1% BSA. After the wash, the cells were pretreated with 1 μ M nisoxetine (TOCRIS, 57754-86-6) in HBSS/BSA for 20 min to suppress NET activity. Dopamine uptake was measured by adding a 1 \times fluorescent dopamine analog (Neurotransmitter Transporter Uptake Assay Kit, Molecular Devices R8173) (16, 17) in HBSS/BSA to the cells in the continuous presence of 1 μ M nisoxetine. The cells were incubated for 15 min at 37°C before observation with a confocal fluorescence microscope at excitation/emission = 440/520 nm for up to 15 min. For DAT inhibition studies, 3 μ M GBR12935 (TOCRIS, 67469-81-2) was incubated instead of nisoxetine. For quantification, the original PC12, PLRP2-KO, and Stx4-KO cells were cultured in 96-well plates and then stimulated with NGF for 72 h. After the application of the dopamine analog in the presence of 1 μ M nisoxetine, as described above, its incorporation into the cells was measured on a microplate fluorometer with excitation/emission = 440/520 nm. For COS7 cells transfected with DAT cDNA constructs, the uptake assays were performed without nisoxetine treatment at 20 h after transfection.

FRET

For the analysis of FRET between DAT and mAb#15, Stx1A and mAb#15, or Stx4 and mAb#15, PC12 cells treated with NGF for 48 h were stained with 3 μ g/ml mAb#15 and either a 1/50-diluted antibody to DAT (Proteintech, 22524-1-AP), a 1/50-diluted antibody to Stx1A (GeneTex, GTX113559), or a 1/50-diluted antibody to Stx4 (GeneTex, GTX114806) in 5% milk, 1% goat serum/PBS, followed by incubation with 1/3,000-diluted secondary antibodies [CF430-labeled antibody to rabbit IgG (Biotium) and Alexa 555-labeled antibody to mouse IgM (Thermo)] in 10% goat serum/PBS. FRET between the two fluorophores was observed with excitation at 440 nm and emission between 630 and 730 nm

using an Olympus FV10 confocal microscope. For the analysis of FRET between mAb#15 and the mCherry-TMD constructs, PC12 cells were stimulated with NGF for 48 h and then transfected with the cDNAs. Cells were fixed at 24 h after transfection and stained with 3 μ g/ml mAb#15 in 5% milk/PBS and 1/5,000-diluted secondary antibody [Alexa 488-labeled antibody to mouse IgM (Thermo) in 1% BSA/PBS]. FRET was observed with excitation at 440 nm and emission between 650 and 700 nm.

Immunoelectron micrograph analyses

PC12 cells (the original, PLRP2-KO, and STX4-KO cells) treated with NGF for 48 h were fixed with 4% paraformaldehyde in 0.1 M sodium phosphate (pH 7.2) for 15 min. After washing with PBS, cells were blocked with 10% goat serum in PBS for 1 h before adding 3 μ g/ml purified mAb#15 IgM and 50-fold-diluted anti-Stx4 or anti-DAT antibodies in 5% skim milk in 1% goat serum in PBS for 12 h at 4°C. After washing the primary antibody with PBS, the cells were stained with a 200-fold-diluted HRP-labeled antibody to mouse IgM (Santa Cruz Biotechnology, SC2064) and a 5-fold-diluted 10 nm colloidal-gold-labeled anti-rabbit IgG (BBI) in 10% goat serum in PBS for 12 h. The localization of mAb#15 was revealed by a DAB substrate kit (Nacalai Tesque, 25985-50). These samples were fixed again with 4% paraformaldehyde in 0.1 M sodium phosphate (pH 7.2) for 15 min and 1% glutaraldehyde in 0.1 M phosphate buffer (pH 7.3) for 10 min at 4°C. They were then postfixed with 1% osmium tetroxide in 0.1 M phosphate buffer (pH 7.3) for 40 min at 4°C and dehydrated in a graded series of ethanol. After dehydration, the cells were embedded in Epon 812 (TAAB Laboratories Equipment Ltd.). Ultrathin sections were observed on a JEM-1230 transmission electron microscope (JEOL, Tokyo, Japan). For the quantification of surface-localized DAT, gold particles were manually counted in four different images of EM at 20,000-fold magnification.

Vesicle immunoprecipitation

The vesicle immunoprecipitation procedure was adapted from previous studies (18, 19). The NFs from the original PC12 cells and the PLRP2-KO cells were homogenized in 1 ml of the lysis buffer with Potter homogenizers at 4°C. The homogenates were centrifuged at 1,000 *g* for 3 min to remove large particles, and the supernatants were used as the neurite vesicle fractions (about 750 μ g of protein each). For vesicle immunoprecipitation, the membrane fractions (200 μ l, 50 μ g of protein each) were adjusted to 0.1 M potassium phosphate (pH 7.4) and incubated with 0.5 μ g of an antibody to Stx4 (Proteintech, 14988-1-AP) for 1 h at 4°C, followed by the addition of 4 μ g of a biotin-labeled antibody to rabbit IgG (SouthernBiotech, 4050-08) to the mix and further incubation for 1 h. Streptavidin-coated magnetic beads (Promega, Z5481) were washed once with blocking buffer [5 mg/ml BSA, 0.1 M potassium phosphate (pH 7.4)] and incubated with the blocking buffer for 2 h. The beads were then washed three times with the blocking buffer and once with the lysis buffer supplemented with 0.1 M potassium phosphate (pH 7.4), and dissolved in this buffer. The beads (150 μ g, 230 μ g/ml) were mixed with the membrane fractions for 12 h at 4°C. The beads were separated from unbound fractions and washed once with lysis buffer supplemented with 0.1 M potassium phosphate (pH 7.4). The bound proteins were eluted by SDS sample buffer [6 M urea, 2% SDS, 10% β -mercaptoethanol, 125 mM Tris (pH 6.8)] for 10 min at 95°C. The protein samples in the fractions were analyzed by Western blotting with an antibody to Thy-1 (Millipore, MAB1406; 1:2500), Stx4 (GeneTex, GTX114806; 1:20,000), DAT (described above), or PLRP2 (described above). The Tidy Blot HRP-reagent (Bio-Rad, STAR209P; 1:5,000 in 5% milk/TBST) was used for the detection of Stx4, DAT, and PLRP2. The secondary antibody for

Thy-1 was an HRP-labeled anti-mouse IgG (Promega, W402B; 1:100,000 in 5% milk/TBST).

RESULTS

Surface biotinylation assay

Surface biotinylation assays were carried out as described previously (20) with Biotin-SS-Sulfo-OSu (Dojin, B572) and streptavidin-coated magnetic beads (Promega, Z5481). Western blotting for DAT was performed as described above. The membrane was stripped with 2% SDS, 0.1 M β -mercaptoethanol, and 62.5 mM Tris (pH 6.8) for 30 min at 55°C, then reprobed with an antibody to ATP1A1 (Na^+/K^+ ATPase; Proteintech, 14418-1-AP) at a 1:20,000 dilution in 5% milk/TBS.

The PLRP2 is the PLA1 that determines OPPC localization

When rat PC12 cells are stimulated with NGF, the cells elongate their neurites and the DAT, which is an integral membrane protein, becomes localized at their tips (12, 21). An immunostaining analysis of these cells using mAb#15, which recognizes OPPC (12), showed its localization at the neurite tips 24 h after the stimulation (Fig. 1A) (12). We previously implicated PLA1 activity in this OPPC localization

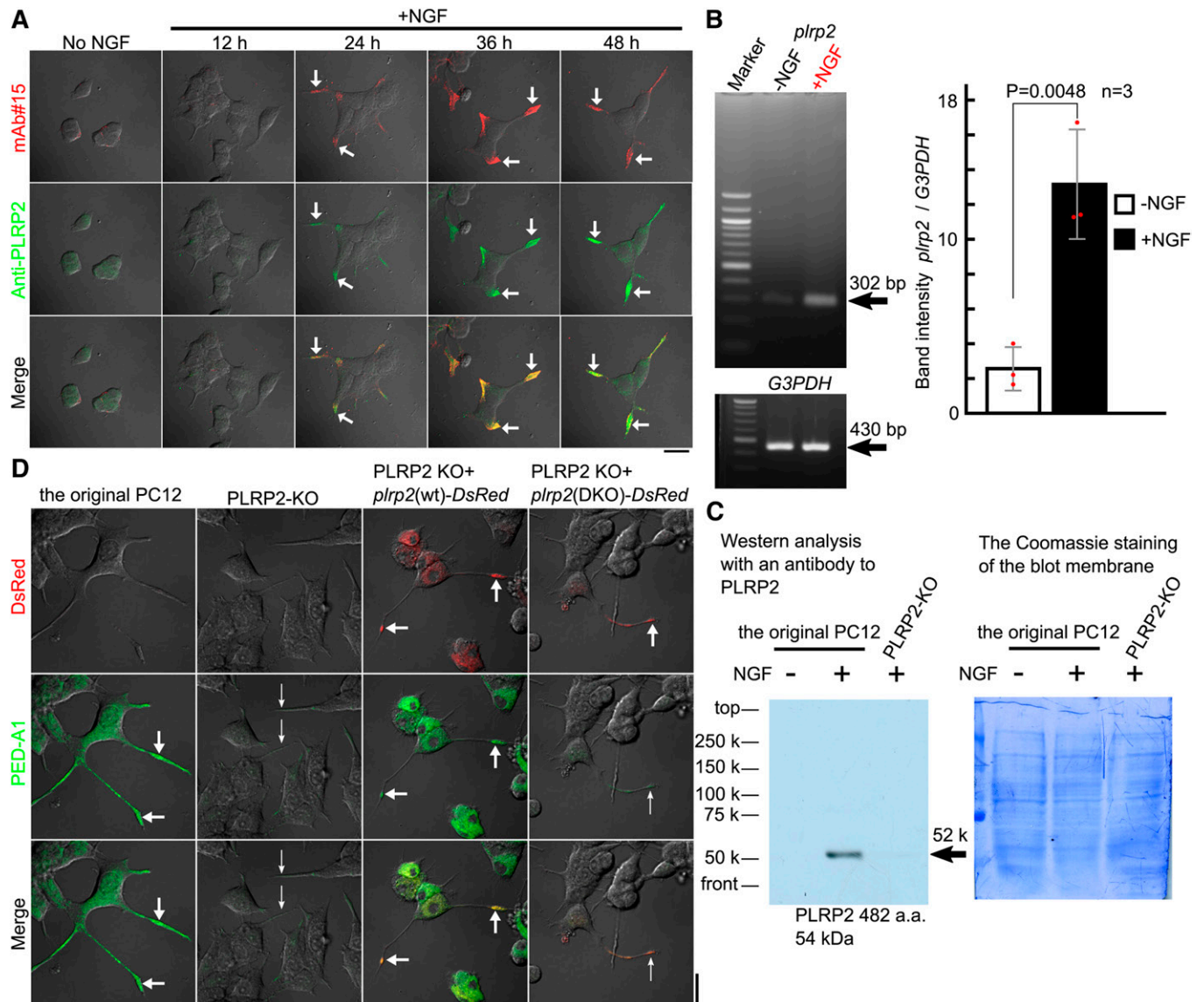


Fig. 1. PLRP2 is the major PLA1 at the tip of PC12 neurites. **A:** PLRP2 colocalized with OPPC during neurite extension in PC12 cells. The cells were immunostained with mAb#15 (red) and an antibody to PLRP2 (green) at 12 h intervals after NGF stimulation. **B:** NGF stimulation induced *plrp2* mRNA expression. PC12 cells were cultured with or without NGF for 48 h and *plrp2* mRNA expression in comparison with *G3PDH* mRNA expression was analyzed by RT-PCR. The band intensities were quantified by ImageJ and statistically analyzed (data are represented as the mean \pm SD, $n = 3$, Student's *t* test). **C:** NGF stimulation induced the PLRP2 protein in PC12 cells. PC12 cells were treated with or without NGF for 48 h and analyzed for PLRP2 protein expression by Western blotting with an antibody to PLRP2. PLRP2-deficient cells (supplemental Fig. S1) with NGF stimulation for 48 h were also analyzed (left). The Coomassie staining of the blot membrane is presented (right). **D:** PLRP2 is the major PLA1 at the tips of PC12 cells. PLA1 activity in the original PC12 and the PLRP2-KO cells was analyzed using a fluorogenic substrate for PLA1 (PED-A1, green). For phenotype-recovery experiments, the wild-type *plrp2* cDNA (wt) or the lipase-inactive form of the *plrp2* cDNA (DKO) were introduced into the KO cells as *DsRed*-labeled forms (red). The heavy arrows and the thin arrows indicate the presence and the absence of the activity, respectively. Scale bars, 20 μm . See also supplemental Fig. S1.

(12); however, the identity of the specific enzyme remained unclear. To address this issue, we screened documented PLA1 enzymes (22) by immunostaining and examined their distribution at the neurite tips. The PLRP2 was localized in these structures (Fig. 1A, Fig. 2A). In addition, it colocalized with OPPC during the extension of neurites (Fig. 1A). An RT-PCR analysis showed that the PLRP2 mRNA was induced by 6.5-fold after NGF stimulation (Fig. 1B). Western blotting also showed that the PLRP2 protein was induced by NGF stimulation (Fig. 1C). These correlations regarding the NGF dependence and the distribution of these molecules suggested the involvement of PLRP2 in OPPC production at the neurite tips.

To examine the roles of PLRP2 in OPPC localization, we edited the *plrp2* (*pnliprp2*) locus in the PC12 genome using the CRISPR/Cas9 system (13). A genome analysis of the resulting IF6 clonal strain showed the successful editing of both loci, which resulted in frameshift mutations (supplemental Fig. S1). The absence of expression of PLRP2 in the strain was verified by both Western blotting (Fig. 1C) and immunostaining (Fig. 2A) with an antibody to PLRP2. Nonetheless, the cells extended neurites after NGF stimulation (Figs. 1D, 2A). PLA1 activity was detected using a fluorogenic substrate, PED-A1 (23), which was present at the tips of neurites in the original PC12 cells (12) but was scarcely detected in the mutant strain (Fig. 1D). This loss of PLA1 activity in the mutant cells was restored by re-expressing

PLRP2 with a DsRed tag (Fig. 1D). In contrast, the replacement of two amino acids in the catalytic core of PLRP2 (24) (184 Ser to Gly and 295 His to Leu) abrogated the rescue of the PLA1 activity (Fig. 1D). These results showed that PLRP2 is the major PLA1 present at the tips of PC12 neurites. In the mutant strain, the immunoreactivity to mAb#15 at the tips of neurites also disappeared (Fig. 2A) but was recovered only when we introduced the wild-type *plrp2* cDNA (Fig. 2A). An LC-MS lipid analysis of the NF of the PLRP2-KO cells showed that OPPC content was significantly decreased to 40% of that of the original PC12 cells (Fig. 2B, supplemental Fig. S2). These data consistently showed that the PLA1 activity of PLRP2 is an essential determinant of the localization of OPPC at the neurite tips. Conversely, ectopic expression of PLRP2-DsRed in COS7 cells (a fibroblast cell line) or in HeLa cells (an epithelial cell line), neither of which produce OPPC naturally (12), led to the formation of OPPC domains together with the enzyme around perinuclear membrane structures (Fig. 2C). These results indicated that the PLA1 activity of PLRP2 is a key determinant of OPPC production and that necessary components after the cleavage are commonly present in these cells as well as in PC12 cells.

PLRP2 is required for DAT localization at the neurite tips

To address the functions of the OPPC domain, we compared the distribution of DAT at the neurite tips between

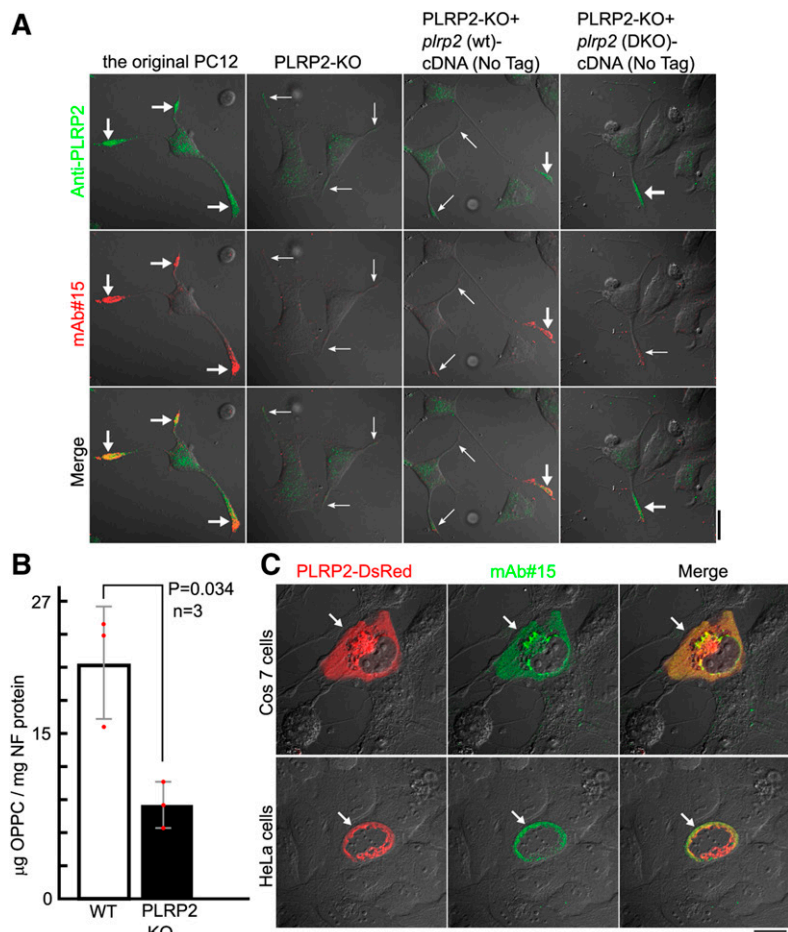


Fig. 2. PLRP2 is the key determinant of OPPC localization at the tip of PC12 neurites. **A:** PLRP2 is necessary for OPPC localization. The original PC12 and the PLRP2-KO cells were immunostained with mAb#15 (red) and an antibody to PLRP2 (green). The wild-type or the lipase-inactive form of the *plrp2* cDNA with no fluorescent tag was introduced into the KO cells for reversion experiments. The heavy arrows and the thin arrows indicate the presence and the absence of the immunostaining, respectively. **B:** Quantification of OPPC in the NFs of the original PC12 and the PLRP2-KO cells. The original PC12 and the PLRP2-KO cells were treated with NGF for 48 h. OPPC content in the NFs was analyzed by LC-MS. Data are represented as the mean \pm SD, $n = 3$, Student's *t*-test. See also supplemental Fig. S2. **C:** The ectopic expression of PLRP2 in nonneuronal cells led to the generation of an OPPC domain around the lipase. The *DsRed*-labeled *plrp2* cDNA was introduced into COS7 cells or into HeLa cells. The localization of OPPC was analyzed by immunostaining with mAb#15 (green). The localization of the lipase was monitored based on the fluorescence of DsRed (red). Scale bars, 20 μ m.

the original PC12 and the PLRP2-deficient cells (Fig. 3A). In contrast to the original cells, in the PLRP2-KO cells, DAT was scarcely detected at the neurite tips or any other part of the cell, although its content in the whole-cell extract did not differ between the two strains (supplemental Fig. S3). These results indicated the dispersed distribution of DAT in the mutant cells. Accordingly, the incorporation of a fluorescent dopamine analog (12, 16, 17) into the neurite tips was also decreased in the PLRP2-KO cells, confirming the absence of DAT localization in these structures (Figs. 3A, supplemental Fig. S4). In addition, the introduction of the *plrp2* cDNA into the PLRP2-KO cells led to

the restoration of both OPPC and DAT at the tips (Fig. 3B). This reversion required the PLA1 activity of PLRP2, as neither OPPC nor DAT was recovered by expressing the lipase-inactive form of the cDNA (Fig. 3B). Notably, the distribution of the Thy-1 protein was not affected in the PLRP2-KO cells (Fig. 3A), showing that the gene disruption affected the localizations of limited proteins. These results showed that the PLA1 activity of PLRP2 is necessary for the distribution of OPPC and for the localization of DAT at the neurite tips. In addition, a FRET analysis showed that DAT and mAb#15 were sufficiently close to produce FRET (25), which revealed that DAT was located

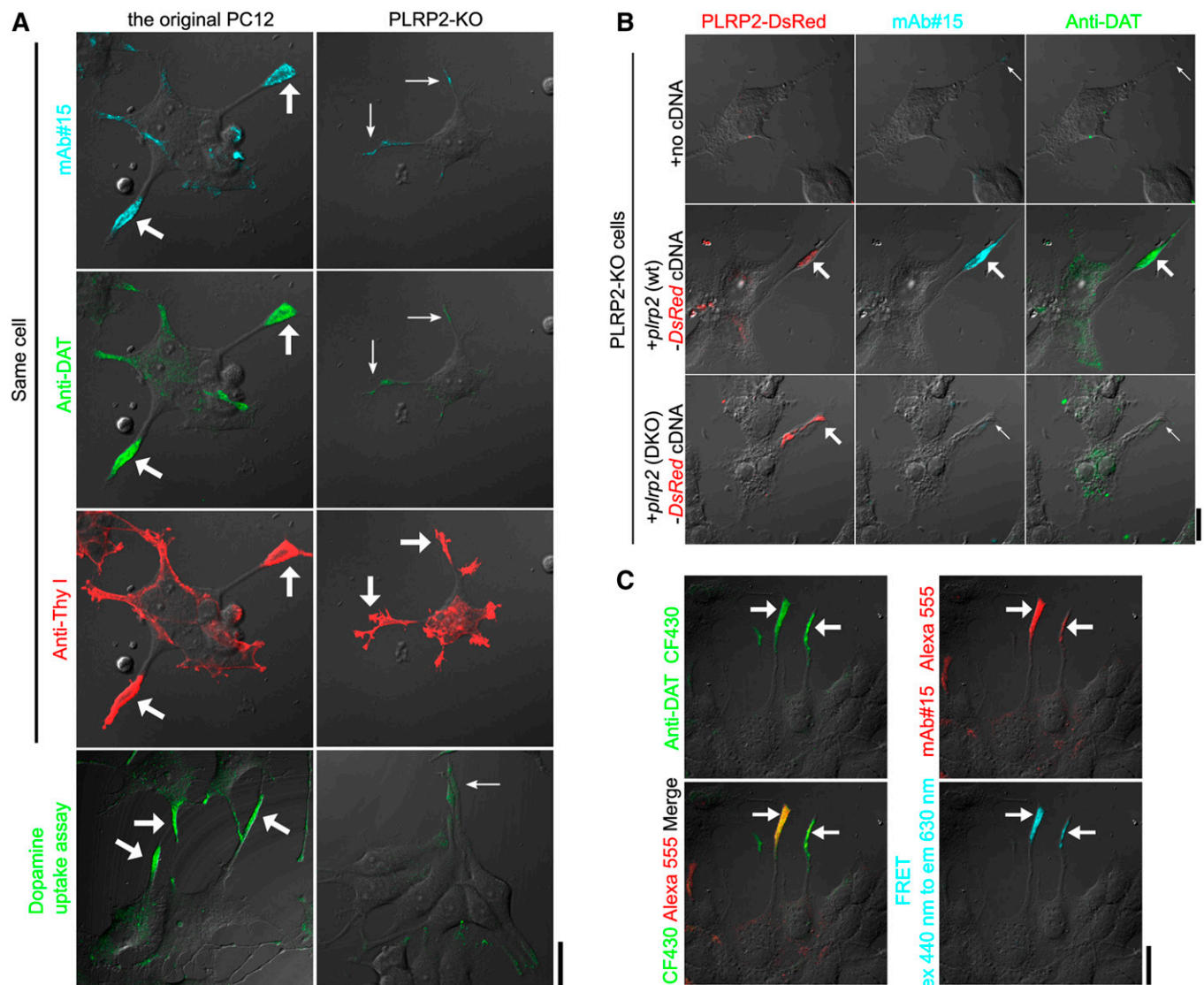


Fig. 3. PLRP2 is required for DAT localization at the neurite tips. **A:** Analysis of DAT localization in the original PC12 and in the PLRP-KO cells. The distribution of OPPC (blue), DAT (green), and Thy-1 (red) was analyzed by immunostaining on the same fixed cells. Using different sets of live cells, the localization of dopamine-uptake activity was analyzed using a fluorescent dopamine analog (green). The specificity of the analog for DAT was analyzed in supplemental Fig. S4. The content of DAT in the whole-cell extracts was analyzed in supplemental Fig. S3. **B:** PLRP2 is required for DAT localization. The distribution of PLRP2-DsRed (red), OPPC (blue), and DAT (green) was analyzed in the PLRP2-KO cells with no addition of cDNA, with the transfection of the wild-type *plrp2*-DsRed cDNA (wt) or of the lipase-inactive *plrp2*-DsRed cDNA (DKO). **C:** OPPC and DAT are located within a distance of 10 nm. NGF-treated PC12 cells were immunostained with mAb#15 (with an Alexa 555-conjugated secondary antibody, red, upper-right panel) and an antibody to DAT (with a CF430-conjugated secondary antibody, green, upper-left panel). The merging of the two images (yellow) is shown in the lower-left panel. FRET from CF430 to Alexa 555 (blue) is shown in the lower-right panel. The heavy arrows and thin arrows indicate the presence and the absence of the activity, respectively. Scale bars, 20 μ m.

within a distance of a few protein molecules from OPPC (Fig. 3C). These results indicated that the allocation of DAT at the neurite tips is controlled by the localization of PLRP2 through a lipid-protein interaction between its reaction product, OPPC, and DAT.

Stx4 forms clusters on the OPPC domain

The results described above indicated that PLRP2 is also involved in the transport of DAT to the neurite tips. To analyze its involvement in vesicular transport, we screened several members of the t-SNARE family by assessing their localizations at the neurite tips via immunostaining. One of these proteins, Stx4, colocalized with OPPC at the tips (Fig. 4B, Fig. 5). In the PLRP2-KO cells, Stx4 was not detected at the tips or any other part of the cell (Figs. 4B and C, 5), although its content in the whole-cell extract did not differ

between the two strains (Fig. 6). These results indicated the diffused distribution of the Stx4 protein in the mutant cells. This lack of Stx4 localization to the neurite tips in PLRP2-KO cells was reversed only by the introduction of the wild-type *plrp2* cDNA into the mutant cells, and not the lipase-inactive form of the cDNA (Fig. 4C). In contrast, Stx1A localized at the more distal tips of the neurites in both the original PC12 and the PLRP2-KO cells (Fig. 4A). Immunoelectron micrograph analysis showed that Stx4 formed clusters on OPPC domains at the cytoplasmic surface of vesicles and of the plasma membrane (Fig. 5). In addition, a FRET analysis showed that Stx4 and mAb#15 were sufficiently close to produce FRET (Fig. 4D). In contrast, FRET was not observed between Stx1A and mAb#15 (Fig. 4D). These results indicated that PLRP2 controls the localization of Stx4 through a lipid-protein interaction via OPPC.

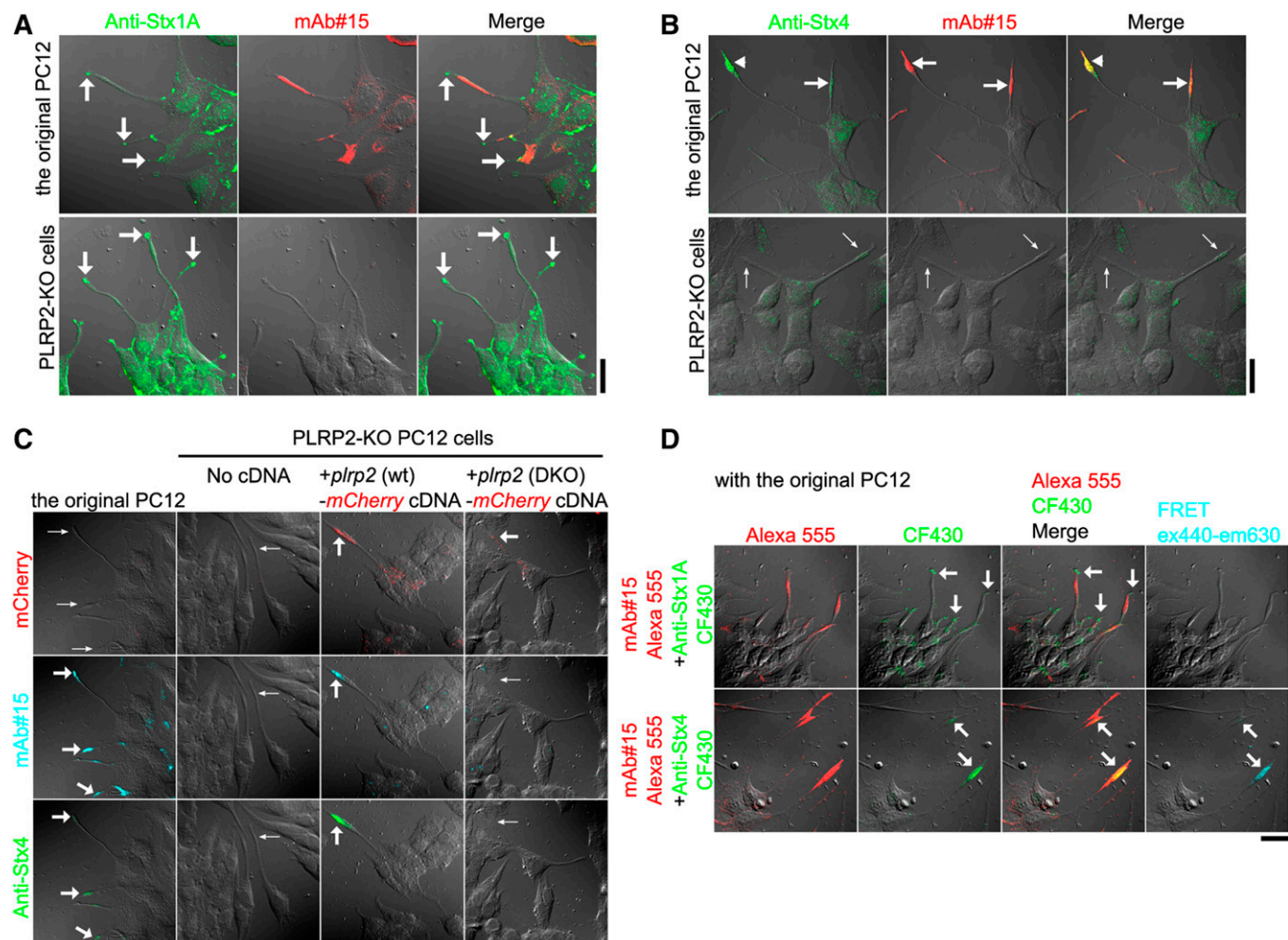


Fig. 4. PLRP2 is necessary for the localization of Stx4 at neurite tips. A, B: Stx4 colocalizes with OPPC at the neurite tips of PC12 cells. The distribution of OPPC (red), Stx1A (A, green), or Stx4 (B, green) was analyzed in the original PC12 or in the PLRP2-KO cells by immunostaining. C: The PLA1 activity of PLRP2 is necessary for the localization of Stx4 at neurite tips. The distribution of OPPC (blue) and Stx4 (green) was analyzed by immunostaining in the original PC12 and the PLRP2-KO cells. In some of the KO cells, the PLRP2-mCherry fusion protein (wt, red) or the lipase-inactive mutant of the PLRP2-mCherry fusion protein (DKO, red) was expressed. D: OPPC and Stx4 are located within a distance of 10 nm. In the upper panel, NGF-treated PC12 cells were immunostained with an antibody to Stx1A (with a CF430-conjugated secondary antibody, green) and with mAb#15 (with an Alexa 555-conjugated secondary antibody, red). In the lower panel, the cells were stained with an antibody to Stx4 (with a CF430-conjugated secondary antibody, green) and with mAb#15 (with an Alexa 555-conjugated secondary antibody, red). FRET from CF430 to Alexa 555 (blue) was analyzed. The heavy arrows and thin arrows indicate the presence and the absence of the activity, respectively. Scale bars, 20 μ m.

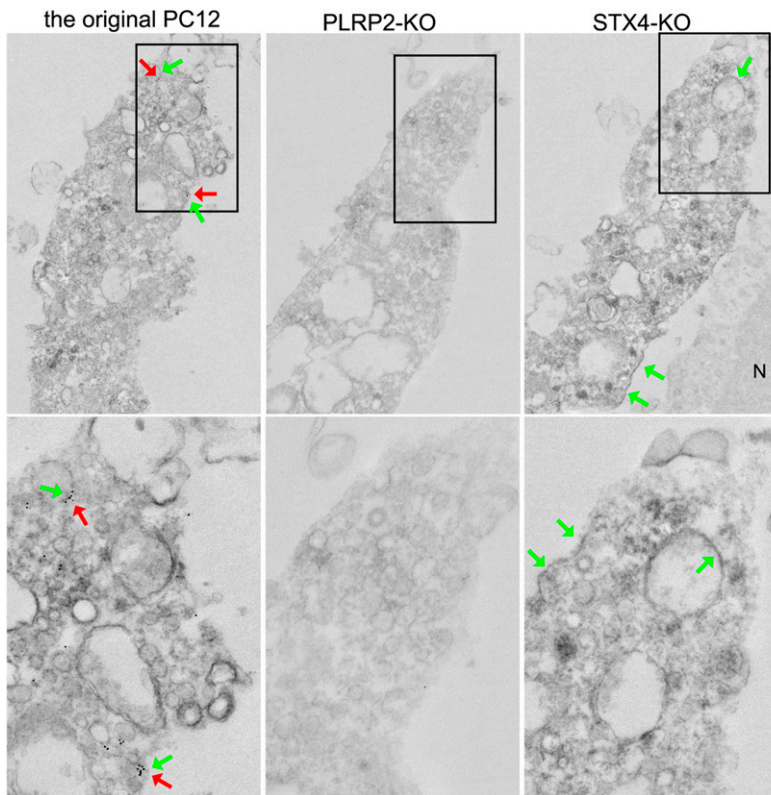


Fig. 5. Stx4 forms clusters on the OPPC domain. Immunoelectron micrograph analysis of the distribution of the OPPC domain (HRP-DAB staining, dense membrane staining, green arrows) and that of Stx4 (10 nm gold particle, red arrows) at the very tip of PC12 cells. Three different genotypes were analyzed: the original PC12 (left), PLRP2-KO (center), and STX4-KO (right) cells. Each area of the rectangles in the upper row is magnified in the lower row. A cell body with a nucleus (labeled with N) of an adjacent cell is shown in the upper-right panel, where mAb#15 staining is absent. Scale bars, 1,000 nm (upper panels) and 400 nm (lower panels).

PLRP2, Stx4, and DAT reside in the same transport vesicles in a PLRP2-dependent manner

The immunostaining analyses described above showed that both Stx4 and DAT are closely localized to OPPC. To analyze the localization of PLRP2, Stx4, and DAT biochem-

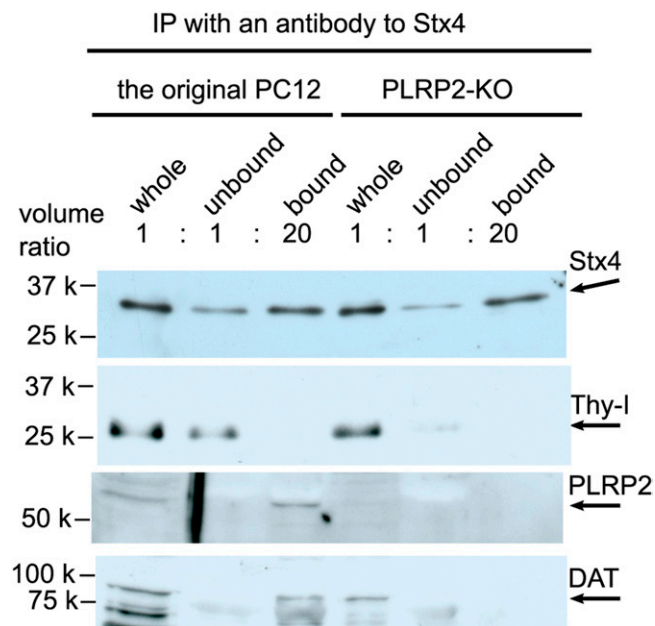


Fig. 6. PLRP2, Stx4, and DAT reside in the same transport vesicles in a PLRP2-dependent manner. The intracellular vesicles in the neurite membrane fraction from the original PC12 or the PLRP2-deficient cells were immunoprecipitated with an antibody to Stx4, and the protein in the bound fractions was analyzed by Western blotting with antibodies to Stx4, Thy-1, PLRP2, or DAT.

ically, we performed vesicle immuno-precipitation assays (18, 19) using an antibody to Stx4 and the original PC12 or the PLRP2-deficient cells (Fig. 6). In the bound fractions, Stx4 was recovered from both the original and the mutant PC12 cells. In contrast, Thy-1 was not recovered in these fractions, showing that Stx4-containing vesicles were selectively enriched in these bound fractions and that Stx4 and Thy-1 did not share transport vesicles. In the bound fraction, both PLRP2 and DAT from the original PC12 cells were enriched. In contrast, from the PLRP2-deficient cells, neither PLRP2 nor DAT was recovered in the bound fraction (Fig. 6). These results showed that PLRP2, Stx4, and DAT reside in the same transport vesicles and that PLRP2 is necessary for assembling these three cargo proteins on the transport vesicles.

An acyl chain-protein interaction between OPPC and the TMD of Stx4 determines the lateral positioning of Stx4 at the plasma membrane

The results reported above indicated that OPPC controls the localization of Stx4 through an acyl chain-protein interaction. Stx1A and Stx4 have their unique TMDs at their carboxy terminals, which greatly facilitates the analysis of this lipid-protein interaction (5). To analyze the roles of TMDs in the localization of these proteins, we appended each TMD to the carboxy terminal of the mCherry fluorescent protein (Fig. 7A). Unmodified mCherry was distributed diffusely throughout the cytoplasm, whereas mCherry-TMD (Stx1A) was localized at the very distal tips of the neurites, both in the original PC12 and in the PLRP2-KO cells (Fig. 7B), similarly to endogenous Stx1A (Fig. 4A). Moreover, mCherry-TMD (Stx4) localized to the tips of neurites only in the original PC12 and not in the PLRP2-KO

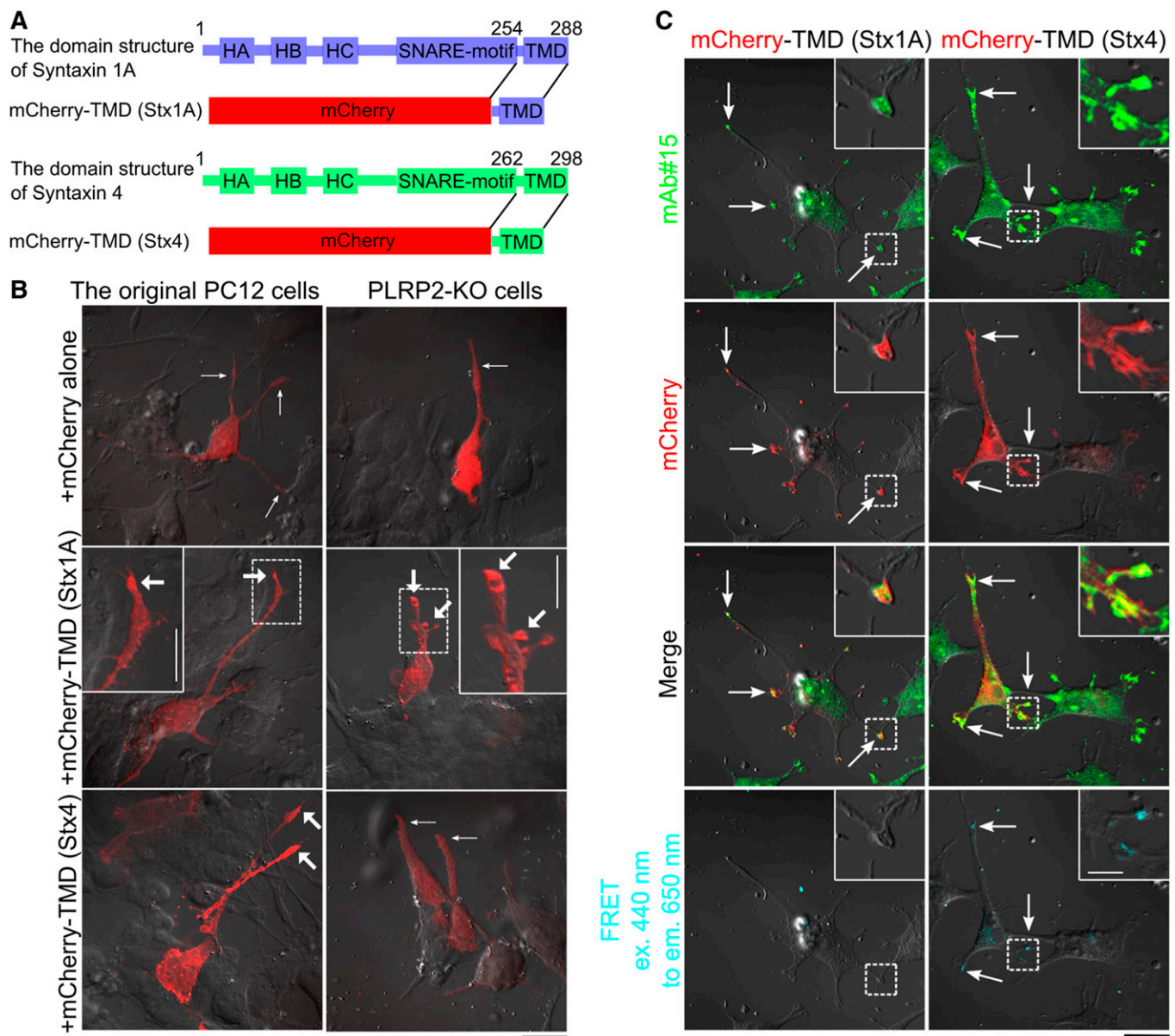


Fig. 7. An acyl chain-protein interaction between OPPC and the TMD of Stx4 determines the lateral positioning of Stx4 at the plasma membrane. **A:** Schematic representation of the fusion constructs of mCherry appended with the TMD of Stx1A or that of Stx4. **B:** The TMDs of Stx1A and Stx4 determine their lateral positioning at the plasma membrane, and the localization of Stx4 to the tips of neurites is dependent on the interaction between its TMD and OPPC. The unmodified mCherry and mCherry-TMD proteins described in **A** were expressed in the original PC12 cells or in the PLRP2-KO cells. The distribution of these mCherry-fusion proteins was observed based on their fluorescence (red). In the figures of mCherry-TMD (Stx1A), the areas in the dashed line were magnified in the insets. The white bars correspond to 10 μ m. The heavy arrows and thin arrows indicate the presence and the absence of the localization, respectively. Scale bars in black, 20 μ m. **C:** OPPC and mCherry-TMD (Stx4) are located within a distance of 10 nm. In the NGF-treated original PC12 cells, mCherry-TMD (Stx1A) (left column) or mCherry-TMD (Stx4) (right column) was expressed. Their distribution in the cells was shown in the second row (red). The cells were immunostained with mAb#15 (with an Alexa 488-conjugated secondary antibody, top row, green). The merging of the two images (yellow) is shown in the third row. FRET from Alexa 488 (excitation at 440 nm) to mCherry (blue, emission at 650 nm) is shown at the bottom. The areas in the dashed line were magnified in the insets. The white bars correspond to 5 μ m. Scale bars in black, 20 μ m.

cells (Fig. 7B). Furthermore, mCherry-TMD (Stx4) and mAb#15 were sufficiently close to provide FRET in the original PC12 cells (Fig. 7C). In contrast, FRET was not observed between mCherry-TMD (Stx1A) and mAb#15 (Fig. 7C). To analyze further the localization mechanism of the TMD, we compared the amino acid sequence of the appended region of Stx4 (rat) with that of six different mammals and with the TMD of Stx1A (rat) (Fig. 8A). Three

amino acid residues within the TMD, i.e., 277A, 284V, and 290I, were conserved across the Stx4 proteins, but not in Stx1A (rat), indicating their functional importance for the tip localization. In fact, in contrast to the wild-type mCherry-TMD (Stx4), the mutant form of the mCherry-TMD (Stx4 290IF), in which isoleucine 290 was replaced with phenylalanine, was distributed around the perinuclear regions and was not localized at the tips of protrusions (Fig. 8B).

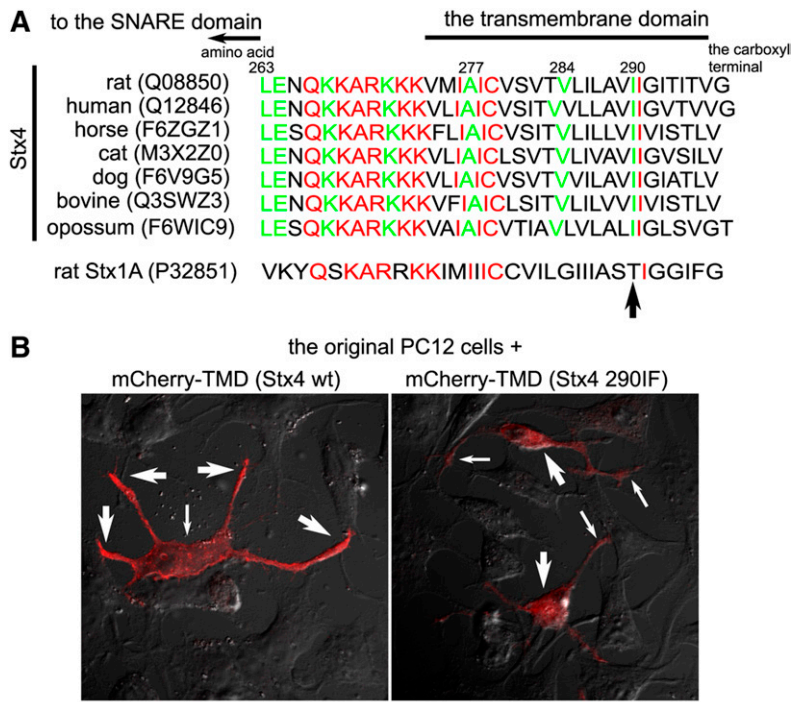


Fig. 8. The conserved Ile at position 290 in the TMD of Stx4 is necessary for its localization at the neurite tips. A: Sequence alignment of the TMDs of Stx4 from seven mammalian species. The amino acid sequences of the TMD of Stx4 from rat, human, horse, cat, dog, bovine, and opossum were compared. In addition, the TMD of rat Stx1A was also aligned. The amino acids that were conserved across all eight sequences are shown in red. The amino acids that were conserved uniquely in Stx4 are presented in green. B: The Ile 290 of Stx4 is necessary for its neurite tip localization. The amino acid corresponding to Ile 290 in mCherry-TMD (Stx4) was changed to Phe to produce mCherry-TMD (Stx4 290IF). This construct and the original mCherry-TMD (Stx4) were expressed in the NGF-treated original PC12 cells. The distribution of these proteins in the cells was observed based on the fluorescence of mCherry (red). The heavy arrows and thin arrows indicate the presence and the absence of the localization, respectively. Scale bar, 20 μ m.

These results indicated that the TMD of Stx1A and that of Stx4 are the determinants of their lateral positioning at the plasma membrane, and that the localization of Stx4 at the tips of neurites is dependent on the sequence-specific interaction of its TMD with the characteristic acyl chain configuration of OPPC.

Stx4 is necessary for the surface expression of DAT

The results described above showed that the localization of both DAT and Stx4 at the neurite tips depends on PLRP2. To address the roles of Stx4 in the localization of PLRP2 or DAT at the tips, we edited the *stx4* locus in the PC12 genome using the CRISPR/Cas9 system (13). A genome analysis of the resulting 2G8 clonal strain confirmed the successful editing of both loci, which resulted in a frameshift mutation and a 228 base insertion that caused the premature termination of the protein (supplemental Fig. S5A). The absence of expression of the Stx4 protein in the strain was verified by Western blotting (supplemental Fig. S5B) and immunostaining analysis (Fig. 5, **Fig. 9A**) using an antibody to Stx4. Nonetheless, the cells extended neurites after NGF stimulation (Figs. 5, 9A, B, and F) and OPPC was still present at the neurite tips (Fig. 9A). These results showed that Stx4 is not necessary for the localization of PLRP2 to the neurite tips. In the Stx4-KO cells, the intensity of the DAT immunostaining at the tips was increased compared with the original PC12 cells (Fig. 9B). However, the incorporation of the fluorescent dopamine analog into the tips was significantly decreased in the Stx4-KO cells (Fig. 9B). Moreover, this deterioration of dopamine incorporation was reversed by expressing the *stx4* cDNA in the cells (Fig. 9F). The quantification of dopamine incorporation into the whole cells showed a significant decrease in the mutant cells, to 34.6% of that of the original cells (Fig. 9C). In addition, surface biotinylation assays (20) revealed

that the surface expression of the DAT protein was significantly decreased both in the PLRP2-KO cells and in the Stx4-KO cells, to 21% and to 37% of that of the original cells, respectively (Fig. 9D, E). Furthermore, an immunoelectron micrograph analysis using an antibody to DAT in Stx4-KO cells showed the increased localization of DAT at the neurite tips compared with the original PC12 cells, although its surface localization was significantly decreased, to 21% of that of the original PC12 cells (**Fig. 10**). These results consistently showed that Stx4 is required for the surface expression of DAT at the neurite tips and that Stx4 is not required during the transport of the vesicles to the vicinity of the target fusion sites at the tips.

Combined expression of PLRP2 and Stx4 enhances the surface expression of DAT in a nonneuronal cell

The results reported above showed that both PLRP2 and Stx4 are necessary for the efficient surface expression of DAT in PC12 cells. To examine whether these two proteins are sufficient for this process, we expressed PLRP2, Stx4, and DAT in COS7 cells at different combinations (**Fig. 11A**). As none of these proteins are naturally expressed in COS7 cells, we expected that the cells would have no specified components to interact with these proteins, while they have a general machinery for the transport of membrane proteins. Thus, we were able to analyze the roles of the OPPC domain and of Stx4 in the surface expression of DAT without the complications of additional factors that are possibly present in neuronal cells. The expression of DAT with mCherry alone using construct #2 led to a negligible detection of DAT by immunostaining (Fig. 11C), although its protein content in the whole-cell extract was the most abundant among the five constructs (Fig. 11B). These results indicated the dispersed distribution of DAT in these cells, as observed in the PLRP2-deficient PC12 cells

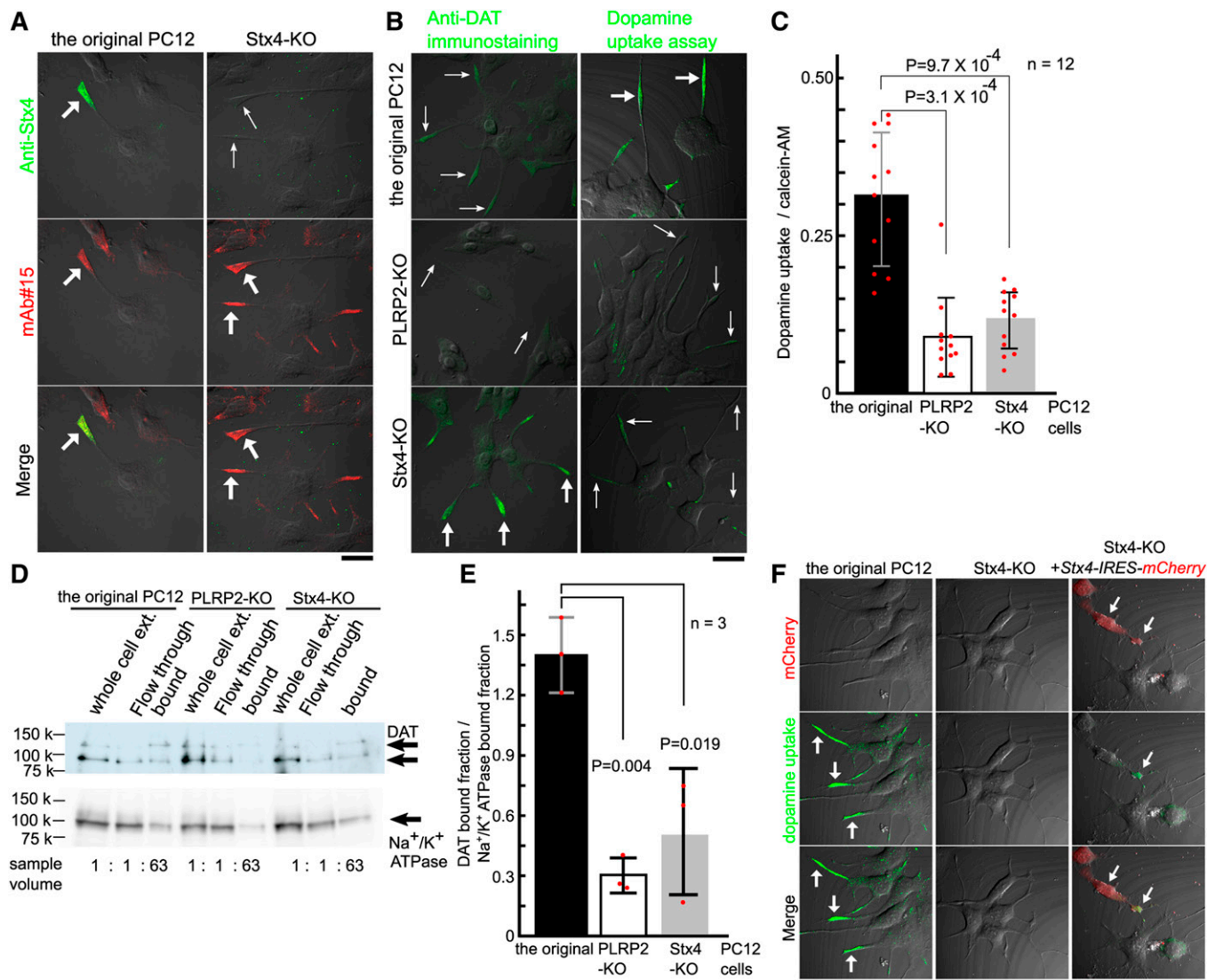


Fig. 9. Stx4 is necessary for the surface expression of DAT. **A:** OPPC localizes at the neurite tips in the absence of Stx4. The distributions of OPPC and Stx4 in the original PC12 and the Stx4-KO cells were analyzed by immunostaining with mAb#15 (red) and an antibody to Stx4 (green). **B:** Stx4 is required for the surface expression of DAT. The distribution of DAT was analyzed by immunostaining in the original PC12, the PLRP2-KO, and the Stx4-KO cells (green, left column). Dopamine-uptake assays were performed in separate sets of these cells (green, right column). The heavy arrows and thin arrows indicate the presence and the absence of the activity, respectively. **C:** Quantification of dopamine uptake by the original PC12, the PLRP2-KO, and the Stx4-KO cells. The cells were cultured in 96-well plates in the presence of NGF for 72 h, and the incorporation of the fluorescent dopamine analog into the cells was quantified by a fluorometer. Data are presented as the mean \pm SD, $n = 12$, Student's *t*-test. **D:** Analysis of DAT surface expression in the original PC12, the PLRP2-KO, and the Stx4-KO cells. Surface biotinylation assays were performed on the three types of cells and the fractions of biotinylated DAT bound to streptavidin beads were analyzed by Western blotting with an antibody to DAT (upper panel). The same blot membrane was re-probed with an antibody to Na⁺/K⁺ ATPase as a positive control for surface expression. **E:** The band intensities of DAT and Na⁺/K⁺ ATPase in (D) were quantified by ImageJ, expressed as the ratio of bound fractions, and statistically analyzed (data are presented as the mean \pm SD, $n = 3$, Student's *t*-test). **F:** Dopamine incorporation into the tip of the Stx4-KO cells was recovered by the re-expression of the *stx4* cDNA. Dopamine incorporation (green) was monitored in the original PC12, the Stx4-KO, or the Stx4-KO cells transfected with the CMV-Stx4-IRES-mCherry cDNA. The cells with successful transfection were indicated by the fluorescence of mCherry (red). The heavy arrows and thin arrows indicate the presence and the absence of the activity, respectively. Scale bars, 20 μ m. See also supplemental Fig. S5.

(Fig. 3A, B, supplemental Fig. S3). In turn, the expression of DAT with the PLRP2-mCherry fusion protein using construct #3 led to the detection of PLRP2 and OPPC at the perinuclear regions, as in Fig. 2C; moreover, DAT was scarcely detected by immunostaining (Fig. 11C). Subsequently, the expression of DAT with mCherry and Stx4 using construct #4 led to the detection of Stx4 at the perinuclear regions, with DAT being scarcely detected by immunostaining

(Fig. 11C). Finally, when DAT was expressed with both PLRP2-mCherry and Stx4 using construct #5, PLRP2, OPPC, and Stx4 were detected most strongly at the tips of cell protrusions, and DAT was detected at the tips and in cell bodies. In addition, its immunostaining was stronger than that detected in the cells transfected with the other constructs (Fig. 11C), although its protein content in the whole-cell extract was the least abundant among the four

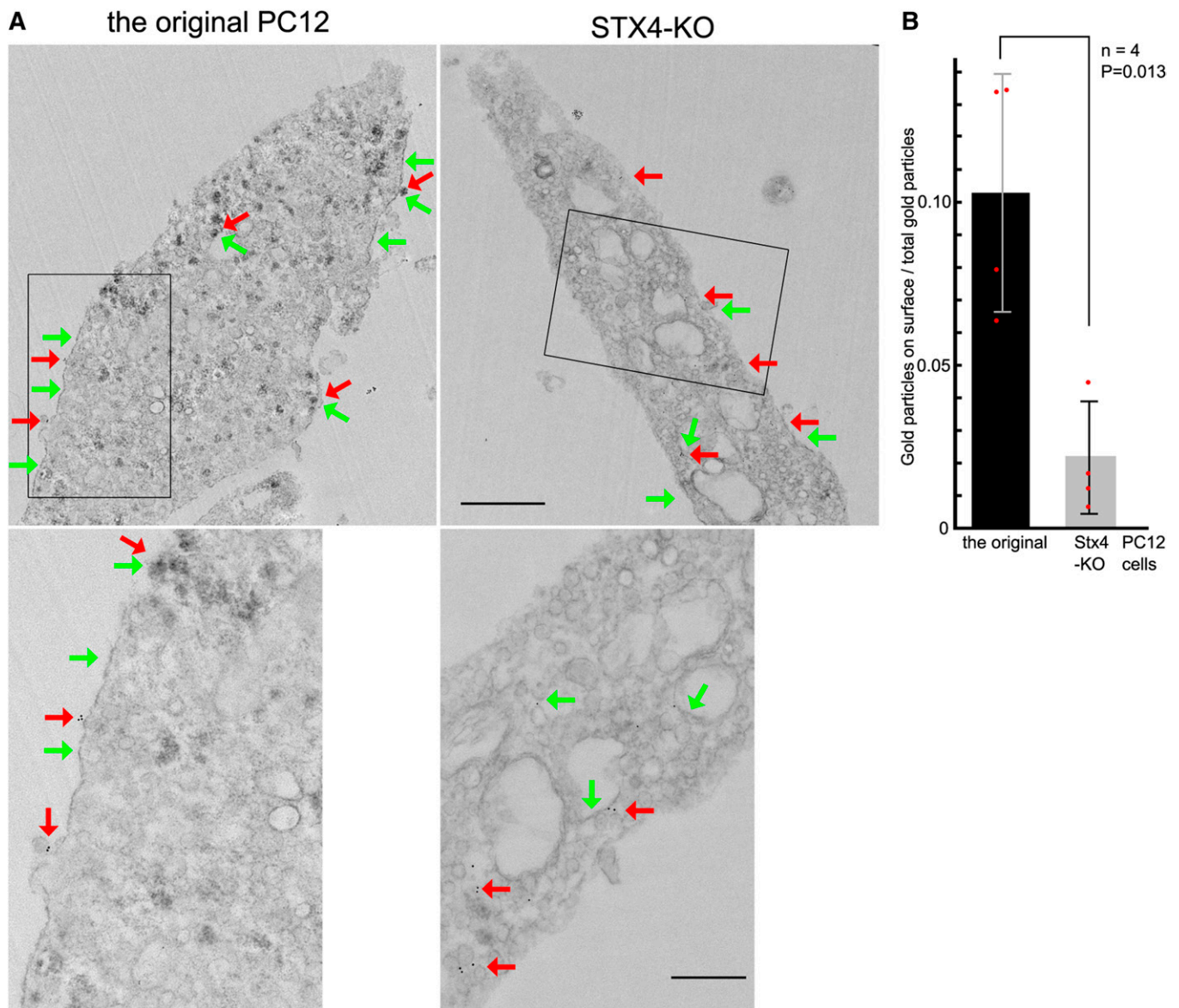


Fig. 10. Immunoelectron micrograph analysis of the distribution of DAT in Stx4-KO cells. A: Distribution of the OPPC domain (HRP-DAB staining, dense membrane staining, green arrows) and that of DAT (10 nm gold particle, red arrows) at the very tip of PC12 cells. The original PC12 (left) and the STX4-KO (right) cells were analyzed. Each area of the rectangle in the upper row is magnified in the lower row. Scale bars, 1,000 nm (upper panels) and 400 nm (lower panels). B: Quantification of the surface expression of DAT by measuring immuno-gold localization. The fraction of surface-localized DAT was analyzed by manually counting immuno-gold localization. Four different micrographs were analyzed for each genotype. The data are presented as the mean \pm SD, $n = 4$, Student's t -test.

constructs that expressed DAT (Fig. 11B). These results indicated that the clustered distribution of the DAT protein took place only in the presence of this latter combination of molecules. Furthermore, using the different conditions mentioned above, we examined the incorporation of the dopamine analog into cells as a measurement of the surface expression of DAT (Fig. 12A, B). Again, the expression of DAT with both PLRP2-mCherry and Stx4 yielded the strongest incorporation, which was significantly increased by 9.1-fold compared with that of the cells transfected with DAT and mCherry alone. These results showed that, even in a nonneuronal cell type, PLRP2 and Stx4 cooperatively facilitated the surface expression of DAT; moreover, they indicated that these two proteins are the central determinants of the transport and surface expression of DAT.

DISCUSSION

Most of the current models of functional segmentation of the plasma membrane rely on structural protein complexes at the border of the domains that provide passive barriers or impedance against the lateral diffusion of membrane proteins (1, 26). Here, we described a distinct mode that depended on enzymatic activity inside the domains, which modified the internal structure of the phospholipid membrane itself.

Although it is known mostly as an extracellular digestive lipase secreted from the pancreas (27), PLRP2 also has PLA1 activity for PC (24) (Fig. 1D), and its transcript is detected in selected areas of the brain (28, 29). In this study, we found that PLRP2 was present at the neurite tips of

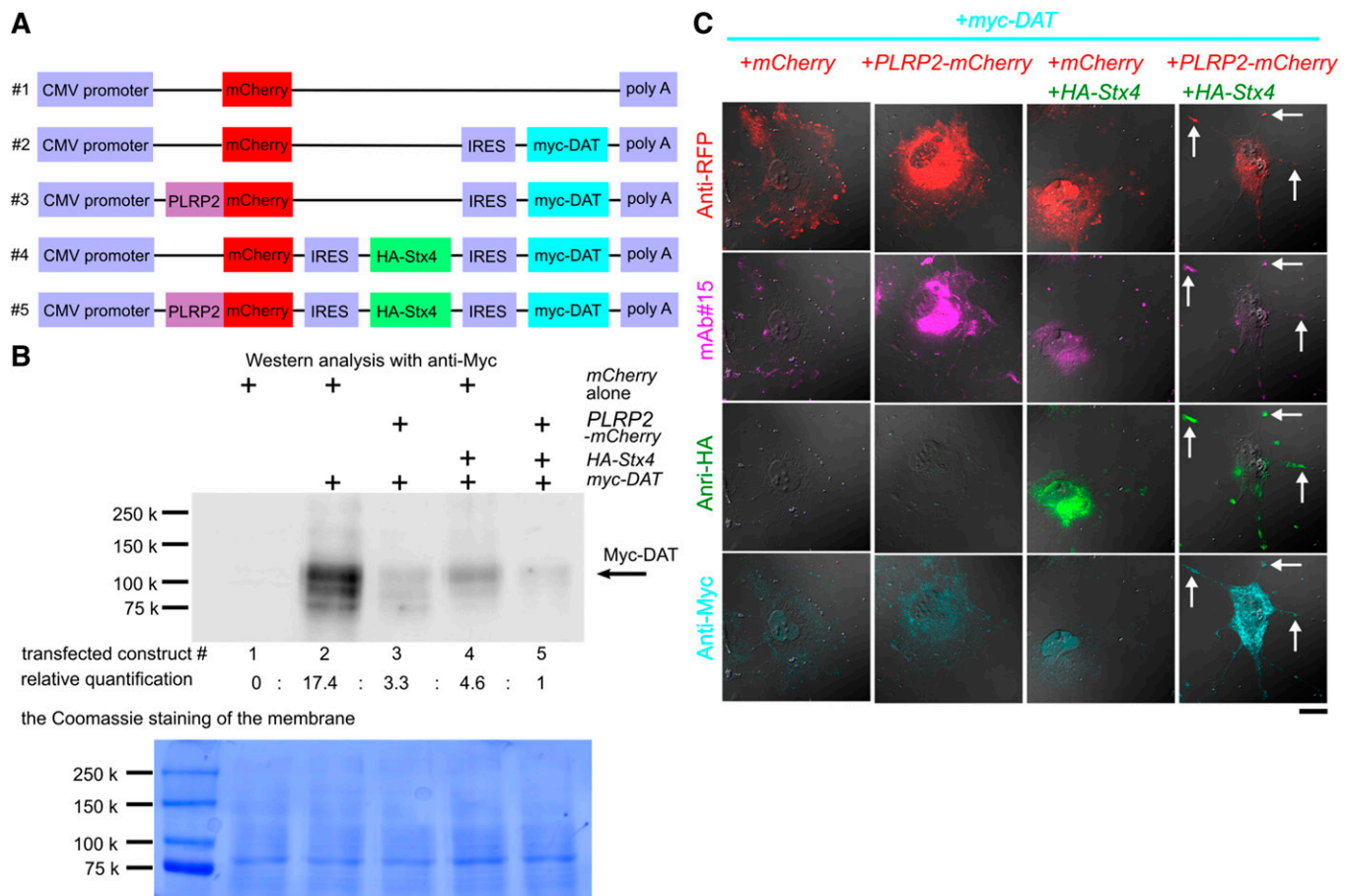


Fig. 11. The combined expression of PLRP2 and Stx4 controls the localization of DAT in a nonneuronal cell. **A:** Schematic illustration of the cDNA expression constructs (#1 to #5) with different combinations of *mCherry*, *plrp2* fused with *mCherry*, *HA*-tagged *stx4*, and *myc*-tagged *DAT*. **B:** Western blot analysis of the expression of the Myc-tagged DAT protein in COS7 cells transfected with the constructs (#1 to #5) detailed in **A**. The blot membrane was probed with an antibody to Myc. The intensities of each band corresponding to Myc-DAT were quantified and are shown relative to that of construct #5 (upper panel). The Coomassie staining of the blot membrane is also shown (lower panel). **C:** Immunostaining analysis on the localization of *mCherry* (red), OPPC (purple), *HA*-Stx4 (green), and Myc-DAT (blue) in COS7 cells transfected with the expression constructs #2 to #5. Scale bar, 20 μ m.

PC12 cells (Figs. 1A, 2A) and that its PLA1 activity was essential for the localization of OPPC at the tips (Fig. 2A, B, supplemental Fig. S2). These results showed that PLRP2 works as a membrane-bound PLA1 in PC12 cells and initiates acyl chain remodeling at the *sn*-1 site of membrane PC, leading to the regional distribution of OPPC. After PLRP2 cleaves the *sn*-1 site, oleic acid must be added back at the site to produce OPPC. Before analyzing its mechanism in detail, we ectopically expressed PLRP2 in COS7 cells or in HeLa cells, which do not express OPPC naturally (12). These ectopic expressions resulted in the production of OPPC around the enzyme (Figs. 2C, 11C), which indicated again that PLRP2 is a key determinant of OPPC localization. In addition, these results implied that the mechanism for adding oleic acid to the *sn*-1 site is generally present among different cell types, despite that there is no report on an acyltransferase that is capable of adding oleic acid to the *sn*-1 site (10, 11). One possible mechanism consistent with this prevalent nature is the spontaneous acyl-migration from the *sn*-2 site to the *sn*-1 site (30). Using abundant 2-oleoyl-PC species, such as 1-palmitoyl-2-oleoyl-PC, as the substrate, PLRP2 initially produces 2-oleoyl-lyso PC, which

is nonenzymatically converted into 1-oleoyl-lyso PC by the acyl-migration. Then, an acyltransferase such as LPCAT1 (31) would add palmitic acid to the *sn*-2 site for completing the OPPC biosynthesis. Further study is required to examine this hypothesis and to identify the acyltransferase involved in the OPPC synthesis.

The PLA1 activity of PLRP2 was essential not only for OPPC localization but also for the localization of DAT and Stx4 at the neurite tips (Figs. 3A and B, 4B and C, 5, 9B). In addition, OPPC was located sufficiently close to provide FRET with DAT and Stx4 (Figs. 3C, 4D, 7C). An immunoelectron micrograph analysis also showed that DAT and Stx4 are located at the OPPC domain (Figs. 5, 10). Moreover, the TMD of Stx4 was sufficient for its correct localization (Fig. 7B, C), which required PLRP2 (Fig. 7B). Furthermore, the isoleucine residue located at position 290 of the TMD of Stx4 was essential for the tip localization of this protein (Fig. 8). These results suggested that the local distribution of OPPC at the tips attracts DAT and Stx4 to the domains through a lipid-protein interaction, albeit the precise mode of interactions between OPPC and these proteins are currently unclear. This lipid

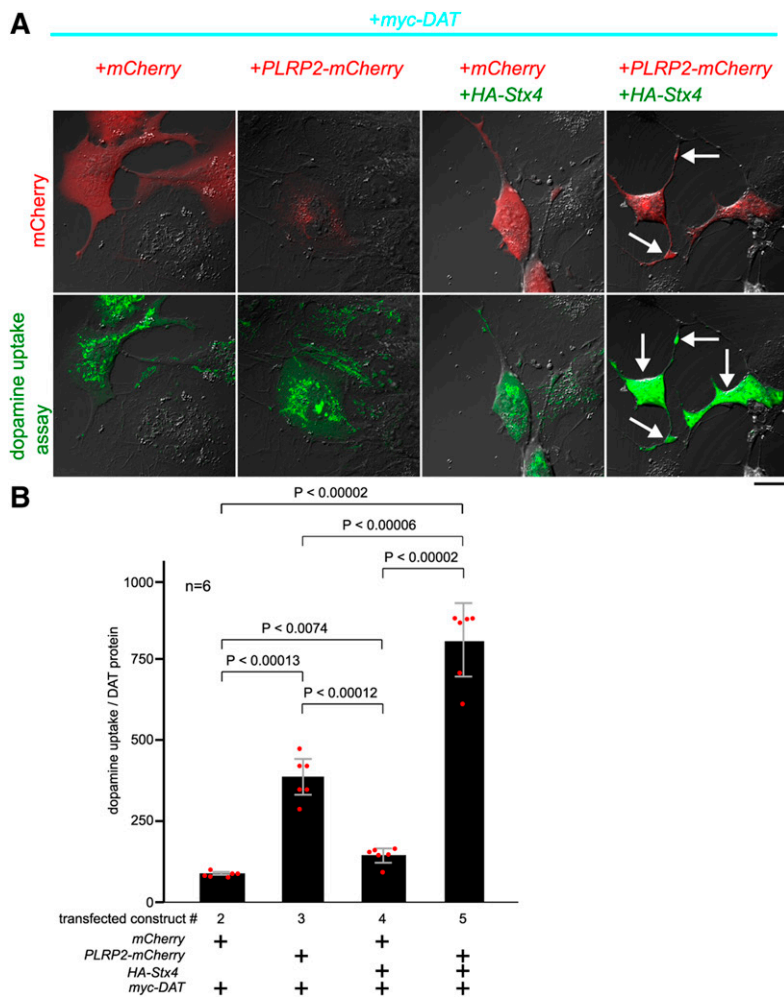


Fig. 12. The combined expression of PLRP2 and Stx4 enhances the surface expression of DAT in a non-neuronal cell. **A:** Dopamine uptake assays in COS7 cells transfected with the expression constructs #2 to #5. The fluorescence of mCherry (red, upper row) and the fluorescence of the incorporated dopamine analog (green, lower row) are shown. Scale bar, 20 μm . **B:** Quantification of dopamine uptake by COS7 cells transfected with the expression constructs #2 to #5. The incorporation of the fluorescent dopamine analog into cells in a 96-well plate that were transfected with constructs #2 to #5 was quantified by a fluorometer and is expressed as dopamine uptake/DAT protein content. Data are presented as the mean \pm SD, $n = 6$, Student's t -test.

domain concept presents a simple and flexible confinement mechanism that does not use barrier structures at the border of the domains. Moreover, this flexibility meets the requirements for the synaptic membranes, where the area of the domains fluctuates according to neuronal activity (32).

In addition to flexibility, the selective nature of its control is a remarkable feature of the acyl-chain domain. In this study, we showed that DAT and Stx4 were controlled by the OPPC domain (Figs. 3A and B, 4B and C, 5, 7B and C, 8, 9B, 11C), whereas Thy-1 and Stx1A were not (Figs. 3A, 4A and D, 7B and C). These results indicated that some proteins selectively recognize the characteristic acyl chain configuration of OPPC and are retained in the domain, while others move freely. This selective nature of the confinement fits the characteristics of the membrane domains found in neurons (3) and possibly provides a basis for the sorting mechanism of membrane proteins in general. Considering the large variety of fatty acid configurations observed in membrane phospholipids (8), it is possible that other phospholipid species with unusual fatty acid configurations form membrane domains at different locations in the cell. In this respect, it is interesting that the TMD of Stx1A was also the determinant of its lateral positioning on the plasma membrane to the very distal tips of neurites (Fig. 7B, C). The identity of the localized lipid counterpart

at the site that is responsible for Stx1A localization will be examined in future studies.

Another feature of the acyl-chain domain is that it links the mechanism of intracellular vesicle transport to that of membrane segmentation at the cell surface. Previous studies have shown that the distribution of several t-SNARE proteins is correlated with functional segments on the plasma membrane (33). However, their causal dependence remains unclear, as the allocation mechanism of t-SNARE is unknown (6). As described above, PLRP2 was necessary for the localization of Stx4, which is a member of t-SNARE that controls selective vesicle fusion to the plasma membrane (5), at the neurite tips (Figs. 4B and C, 5, 7B), while Stx4 was not essential for the localization of PLRP2 at the tips (Fig. 9A). In addition, both PLRP2 and Stx4 were necessary for the efficient surface expression of DAT in PC12 cells (Figs. 9, 10), as well as in COS7 cells expressing DAT ectopically (Fig. 12). Furthermore, PLRP2 was necessary for the formation of the transport vesicles that carried both Stx4 and DAT (Fig. 6). These results suggest that the OPPC localization afforded by localized PLRP2 is the primary cause of the Stx4 localization at the tips. This localized Stx4 protein facilitated the fusion of the transport vesicles that carry DAT to the domain of the plasma membrane (Figs. 9, 10), leading to the localized distribution of the transporter at this region. This mechanism

presents the vesicle fusion machinery as another integral component of the plasma membrane segmentation. The identity of the corresponding v-SNARE on the transport vesicles and the initial localization mechanism of PLRP2 to the tips remained unidentified in this study.

We identified two key proteins involved in the allocation control of DAT. The first was PLRP2, which was required consistently in the different stages of the process, from the formation of its transport vesicles (Fig. 6) to its confinement within the limited region of the plasma membrane (Figs. 3, 9B, 11). The second was Stx4, which was necessary for its efficient surface expression at the neurite tips (Figs. 9, 10). As several neuronal disorders are linked to localization anomalies of DAT (34–36), these findings might offer new clues for understanding the mechanisms of such disorders. In previous studies, although its functional significance remains controversial (37, 38), a direct protein-protein interaction between DAT and Stx1A has been described (39), which is inconsistent with our results in terms of the distinct distribution of DAT and Stx1A in PC12 cells (Fig. 4) and in terms of the functional interaction between DAT and Stx4 (Figs. 9–12). Further studies are needed to analyze these discrepancies.

Here, we presented a mechanism of membrane protein localization that was dependent on PLA1, an acyl chain-protein interaction, and the vesicle fusion machinery. The PLA1 enzyme produces the regional distribution of one particular molecular species of phospholipid to attract target membrane proteins through an acyl chain-protein interaction. Using this lipid-protein interaction, the corresponding t-SNARE also positioned itself at the region through its TMD. This t-SNARE localization, in turn, promoted the selective delivery of target proteins to form functional domains at the sites. As discussed above, this mechanism is widely and seamlessly applicable to the sorting, the selective transport, and the selective confinement of membrane proteins. Furthermore, as phospholipid remodeling is a universal process in cells (7), it is likely that cells other than neurons also use this mechanism. Thus, it will be fruitful to study the involvement of PLRP2 or other members of the PLA1 family in various cellular functions that require allocation control of membrane proteins

Data availability

All data are contained within the article. 



Acknowledgments

The authors thank T. Taguchi at Tohoku University for suggestions on detergent techniques for the immunostaining analysis of lipids and M. Shudou at Ehime University for support with EM study.

Author contributions

H.K. experiments; I.M. DAT cDNA cloning and experiments; K.Y. electron micrography experiments; K.H. research design; H.K. and K.H. writing.

Author ORCIDs

Hideaki Kuge  <https://orcid.org/0000-0001-6202-9202>;
Koichi Honke  <https://orcid.org/0000-0002-6123-7576>

Funding and additional information

This work was supported in part by Ono Pharmaceutical (Osaka, Japan).

Conflict of interest

The authors declare that they have no conflicts of interest with the contents of this article.

Abbreviations

DAT, dopamine transporter; G3PDH, glycerol-3-phosphate dehydrogenase; NF, neurite fraction; NGF, nerve growth factor; OPPC, 1-oleoyl-2-palmitoyl-PC; PLA1, phospholipase A1; PLRP2, pancreatic lipase-related protein 2; SNARE, soluble N-ethylmaleimide-sensitive factor attachment protein receptor; Stx1A, syntaxin 1A; Stx4, syntaxin 4; TMD, transmembrane domain; t-SNARE, target-soluble N-ethylmaleimide-sensitive factor attachment protein receptor; v-SNARE, vesicular-soluble N-ethylmaleimide-sensitive factor attachment protein receptor.

Manuscript received August 14, 2020, and in revised form September 11, 2020. Published, JLR Papers in Press, September 22, 2020, DOI 10.1194/jlr.RA120001087.

REFERENCES

1. Caudron, F., and Y. Barral. 2009. Septins and the lateral compartmentalization of eukaryotic membranes. *Dev. Cell.* **16**: 493–506.
2. Horton, A. C., and M. D. Ehlers. 2003. Neuronal polarity and trafficking. *Neuron.* **40**: 277–295.
3. Fukano, T., H. Hama, and A. Miyawaki. 2004. Similar diffusibility of membrane proteins across the axon-soma and dendrite-soma boundaries revealed by a novel FRAP technique. *J. Struct. Biol.* **147**: 12–18.
4. Rodriguez-Boulan, E., G. Kreitzer, and A. Müsch. 2005. Organization of vesicular trafficking in epithelia. *Nat. Rev. Mol. Cell Biol.* **6**: 233–247.
5. Jahn, R., and R. H. Scheller. 2006. SNAREs - engines for membrane fusion. *Nat. Rev. Mol. Cell Biol.* **7**: 631–643.
6. Wang, T., L. Li, and W. Hong. 2017. SNARE proteins in membrane trafficking. *Traffic.* **18**: 767–775.
7. Hermansson, M., K. Hokynar, and P. Somerharju. 2011. Mechanisms of glycerophospholipid homeostasis in mammalian cells. *Prog. Lipid Res.* **50**: 240–257.
8. Taguchi, R., and M. Ishikawa. 2010. Precise and global identification of phospholipid molecular species by an Orbitrap mass spectrometer and automated search engine Lipid Search. *J. Chromatogr. A.* **1217**: 4229–4239.
9. Lands, W. E. 1958. Metabolism of glycerolipides; a comparison of lecithin and triglyceride synthesis. *J. Biol. Chem.* **231**: 883–888.
10. Shindou, H., D. Hishikawa, T. Harayama, K. Yuki, and T. Shimizu. 2009. Recent progress on acyl CoA: lysophospholipid acyltransferase research. *J. Lipid Res.* **50** (Suppl.): S46–S51.
11. Yamashita, A., Y. Hayashi, Y. Nemoto-sasaki, M. Ito, S. Oka, T. Tanikawa, K. Waku, and T. Sugiura. 2014. Progress in Lipid Research Acyltransferases and transacylases that determine the fatty acid composition of glycerolipids and the metabolism of bioactive lipid mediators in mammalian cells and model organisms. *Prog. Lipid Res.* **53**: 18–81.
12. Kuge, H., K. Akahori, K. I. Yagyu, and K. Honke. 2014. Functional compartmentalization of the plasma membrane of neurons by a unique acyl chain composition of phospholipids. *J. Biol. Chem.* **289**: 26783–26793.
13. Sanjana, N. E., O. Shalem, and F. Zhang. 2014. Improved vectors and genome-wide libraries for CRISPR screening. *Nat. Methods.* **11**: 783–784.

14. Hsu, F. F., A. Bohrer, and J. Turk. 1998. Formation of lithiated adducts of glycerophosphocholine lipids facilitates their identification by electrospray ionization tandem mass spectrometry. *J. Am. Soc. Mass Spectrom.* **9**: 516–526.
15. Al-Saad, K. A., W. F. Siems, H. H. Hill, V. Zabrouskov, and N. R. Knowles. 2003. Structural analysis of phosphatidylcholines by post-source decay matrix-assisted laser desorption/ionization time-of-flight mass spectrometry. *J. Am. Soc. Mass Spectrom.* **14**: 373–382.
16. Schwartz, J. W., R. D. Blakely, and L. J. DeFelice. 2003. Binding and transport in norepinephrine transporters: Real-time, spatially resolved analysis in single cells using a fluorescent substrate. *J. Biol. Chem.* **278**: 9768–9777.
17. Mason, J. N., H. Farmer, I. D. Tomlinson, J. W. Schwartz, V. Savchenko, L. J. DeFelice, S. J. Rosenthal, and R. D. Blakely. 2005. Novel fluorescence-based approaches for the study of biogenic amine transporter localization, activity, and regulation. *J. Neurosci. Methods.* **143**: 3–25.
18. Morciano, M., J. Burré, C. Corvey, M. Karas, H. Zimmermann, and W. Volkandt. 2005. Immunoisolation of two synaptic vesicle pools from synaptosomes: A proteomics analysis. *J. Neurochem.* **95**: 1732–1745.
19. Volchuk, A., R. Sargeant, S. Sumitani, Z. Liu, L. He, and A. Klip. 1995. Cellubrevin is a resident protein of insulin-sensitive GLUT4 glucose transporter vesicles in 3T3-L1 adipocytes. *J. Biol. Chem.* **270**: 8233–8240.
20. Witting, S. R., J. N. Maiorano, and W. S. Davidson. 2003. Ceramide enhances cholesterol efflux to apolipoprotein A-I by increasing the cell surface presence of ATP-binding cassette transporter A1. *J. Biol. Chem.* **278**: 40121–40127.
21. Kadota, T., T. Yamaai, Y. Saito, Y. Akita, S. Kawashima, K. Moroi, N. Inagaki, and K. Kadota. 1996. Expression of dopamine transporter at the tips of growing neurites of PC12 cells. *J. Histochem. Cytochem.* **44**: 989–996.
22. Aoki, J., A. Inoue, K. Makide, N. Saiki, and H. Arai. 2007. Structure and function of extracellular phospholipase A1 belonging to the pancreatic lipase gene family. *Biochimie.* **89**: 197–204.
23. Darrow, A. L., M. W. Olson, H. Xin, S. L. Burke, C. Smith, C. Schalk-Hihi, R. Williams, S. S. Bayoumy, I. C. Deckman, M. J. Todd, et al. 2011. A novel fluorogenic substrate for the measurement of endothelial lipase activity. *J. Lipid Res.* **52**: 374–382.
24. Withers-Martinez, C., F. Carrière, R. Verger, D. Bourgeois, and C. Cambillau. 1996. A pancreatic lipase with a phospholipase A1 activity: Crystal structure of a chimeric pancreatic lipase-related protein 2 from guinea pig. *Structure.* **4**: 1363–1374.
25. Shrestha, D., A. Jenei, P. Nagy, G. Vereb, and J. Szöllösi. 2015. Understanding FRET as a research tool for cellular studies. *Int. J. Mol. Sci.* **16**: 6718–6756.
26. Krapf, D. 2018. Compartmentalization of the plasma membrane. *Curr. Opin. Cell Biol.* **53**: 15–21.
27. Andersson, L., F. Carrière, M. E. Lowe, A. Nilsson, and R. Verger. 1996. Pancreatic lipase-related protein 2 but not classical pancreatic lipase hydrolyzes galactolipids. *Biochim. Biophys. Acta.* **1302**: 236–240.
28. Lein, E. S., M. J. Hawrylycz, N. Ao, M. Ayres, A. Bensinger, A. Bernard, A. F. Boe, M. S. Boguski, K. S. Brockway, E. J. Byrnes, et al. 2007. Genome-wide atlas of gene expression in the adult mouse brain. *Nature.* **445**: 168–176.
29. Allen Institute for Brain Science. Allen Mouse Brain Atlas: Available from: <https://mouse.brain-map.org/experiment/show/69816362>.
30. Plückthun, A., and E. A. Dennis. 1982. Acyl and phosphoryl migration in lysophospholipids: importance in phospholipid synthesis and phospholipase specificity. *Biochemistry.* **21**: 1743–1750.
31. Nakanishi, H., H. Shindou, D. Hishikawa, T. Harayama, R. Ogasawara, A. Suwabe, R. Taguchi, and T. Shimizu. 2006. Cloning and characterization of mouse lung-type acyl-CoA: lysophosphatidylcholine acyltransferase 1 (LPCAT1): Expression in alveolar type II cells and possible involvement in surfactant production. *J. Biol. Chem.* **281**: 20140–20147.
32. Choquet, D., and A. Triller. 2013. The dynamic synapse. *Neuron.* **80**: 691–703.
33. Low, S. H., S. J. Chapin, T. Weimbs, L. G. Kömüves, M. K. Bennett, and K. E. Mostov. 1996. Differential localization of syntaxin isoforms in polarized Madin-Darby canine kidney cells. *Mol. Biol. Cell.* **7**: 2007–2018.
34. Sakrikar, D., M. S. Mazei-Robison, M. A. Mergy, N. W. Richtand, Q. Han, P. J. Hamilton, E. Bowton, A. Galli, J. Veenstra-VanderWeele, M. Gill, et al. 2012. Attention deficit/hyperactivity disorder-derived coding variation in the dopamine transporter disrupts microdomain targeting and trafficking regulation. *J. Neurosci.* **32**: 5385–5397.
35. Kovtun, O., D. Sakrikar, I. D. Tomlinson, J. C. Chang, X. Arzeta-Ferrer, R. D. Blakely, and S. J. Rosenthal. 2015. Single-quantum-dot tracking reveals altered membrane dynamics of an attention-deficit/hyperactivity-disorder-derived dopamine transporter coding variant. *ACS Chem. Neurosci.* **6**: 526–534.
36. Kurian, M. A., J. Zhen, S. Cheng, Y. Li, S. R. Mordekar, P. Jardine, N. V. Morgan, E. Meyer, L. Tee, S. Pasha, et al. 2009. Homozygous loss-of-function mutations in the gene encoding the dopamine transporter are associated with infantile parkinsonism-dystonia. *J. Clin. Invest.* **119**: 1595–1603.
37. Fujiwara, T., M. Snada, T. Kofuji, T. Yoshikawa, and K. Akagawa. 2010. HPC-1/syntaxin 1A gene knockout mice show abnormal behavior possibly related to a disruption in 5-HTergic systems. *Eur. J. Neurosci.* **32**: 99–107.
38. Cervinski, M. A., J. D. Foster, and R. A. Vaughan. 2010. Syntaxin 1A regulates dopamine transporter activity, phosphorylation and surface expression. *Neuroscience.* **170**: 408–416.
39. Lee, K. H., M. Y. Kim, D. H. Kim, and Y. S. Lee. 2004. Syntaxin 1A and receptor for activated C kinase interact with the N-terminal region of human dopamine transporter. *Neurochem. Res.* **29**: 1405–1409.